Geomorphology 440 (2023) 108864

Contents lists available at ScienceDirect

Geomorphology

journal homepage: www.journals.elsevier.com/geomorphology

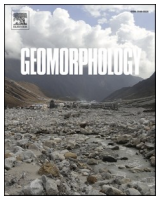

Reconstructing depositional environments through cave interior facies: The case of Galería Complex (Sierra de Atapuerca, Spain)

I. Campaña [a,*], A. Benito-Calvo [b], A. Pérez-González [c], A.I. Ortega [b], A. Álvaro-Gallo [b], L. Miguens-Rodríguez [b], J. Iglesias-Cibanal [b], J.M. Bermúdez de Castro [b], E. Carbonell [d,e]

[a] Departamento de Ecología y Geología, Facultad de Ciencias, Universidad de Málaga, Campo de teatinos s/n, 29071 Málaga, Spain
[b] Centro Nacional de Investigación Sobre Evolución Humana (CENIEH), Paseo de la Sierra de Atapuerca 3, 09002 Burgos, Spain
[c] Instituto de Evolución en Africa-IDEA, Covarrubias 36, 28010 Madrid, Spain
[d] Universitat Rovira i Virgili, Departament d'Història i Història de l'Art, Avinguda de Catalunya 35, 43002 Tarragona, Spain
[e] Institut Català de Paleoecologia Humana I Evolució Social (IPHES-CERCA), Tarragona, Spain

ARTICLE INFO

Keywords:
Early Pleistocene
Atapuerca
Cave sedimentation
Sedimentary facies
Interior facies

ABSTRACT

This work showed that cave sediments are useful for geomorphologic studies and for reconstructing depositional environments. While the cave entrance facies have been extensively studied for their relationship with the fossil and archaeological record, the cave interior facies have received much less attention, although they can provide much information on the geomorphological evolution of the karst. This work presents the stratigraphic and sedimentological study of a section >6 m thick and 10 m long of cave interior sediments of Galería Complex (Sierra de Atapuerca, Spain). Galería Complex is a cavity infill of the Sierra de Atapuerca (Spain), composed of three sections filled by at least 30 m of Pleistocene sediments. This sequence is divided into 5 lithostratigraphic units named from bottom to top: GI – GV. GI unit is 19 m thick of interior facies in the base of the Galería Complex, divided into two sub-unit, GIa and GIb, by the Matuyama-Bruhnes paleomagnetic boundary. GI unit shows an issue with the chronology since has uncoherent between TT-OSL and ESR/U-series and paleomagnetism dates. This work has been done by combining field observation with laboratory sedimentary analysis to characterize the texture and structure of the sediments. Based on these studies, 12 layers and 9 sedimentary facies have been identified. The facies associations indicate a clear separation between GIa and GIb sub-units. GIa sub-unit is dominated by epiphreatic conditions and represents continuous relativity sedimentation during the Early Pleistocene; meanwhile, GIb shows important erosion events and facies with reworked materials that indicate vadose conditions during the Middle Pleistocene. This environmental change is related to the geomorphological evolution of the Arlanzón River. In addition, soft-sediment deformation structures have been described, including faults and low-angle folds. An important leaching process has been identified by the presence of phosphates that could explain the underestimated ages obtained in other works.

1. Introduction

Cave sedimentary infills have been well studied as they often provide valuable information for the evolution of the landscape and the environment of karst area (Farrand, 2001; Kadlec et al., 2008; Arriolabengoa et al., 2015, Martini et al., 2018; Kampolis et al., 2022 among others). The sedimentary processes that fill a cave are related to hydrological and environmental changes both from the outside, i.e. fluvial incision, and from the inside, i.e. collapse, the shape of the cave. The stratigraphic record inside a cave can work as paleoenvironment records since the caves can act as sediment traps (Farrand, 2001); that is, the sediment inside a cave is not affected by the outside erosional processes. Identifying the different sedimentary facies from karst infills helps reconstruct the sequence of processes that occurred in the formation of the cavities, their evolution, which can be polygenic, their abandonment and fossilization, and their relationship between archaeological accumulations and sediments (Farrand, 1975; Goldberg and Sherwood, 2006; Stratford et al., 2022).

Caves work as small, confined sedimentary basins where erosion and deposition processes can occur on a small scale. Thus, sedimentary

* Corresponding author.
E-mail address: i.campanna.lozano@gmail.com (I. Campaña).

https://doi.org/10.1016/j.geomorph.2023.108864
Received 2 February 2023; Received in revised form 19 July 2023; Accepted 9 August 2023
Available online 15 August 2023

inputs are accommodated to the space available within the cavity, and sedimentary facies that in the exterior would be a magnitude of tens of meters, in these environments may occupy only a few meters. In this context, the law of superposition of strata is sometimes not fulfilled in the karst sedimentary record due to landslides, reworking, erosion, hanging sediments, declogging, or other geological processes (Osborn, 1984).

The source of the cave sediments is diverse. Several attempts have been made to classify the cave sediments. One of these first attempts was proposed by Kukla and Lozek (1958), that noted that the sedimentological dynamics inside a cave or karst system are different depending on the distance to the entrance. Therefore, these authors have differentiated between the sediments derived from the interior cave dynamics, so-called interior facies, and others coming from the outside and introduced into the cavity through natural entrances, so-called entrance facies. This classification has been used in different works, including recent ones (Creer and Kopper, 1976; Šroubek et al., 2007; Campaña et al., 2022). Entrance facies mainly consist of clastic sediments derived from soil washed down hillslopes and rock fragments transported by gravity, streams, or wind. These sediments can include animals and human remains that are preserved inside the cave. Therefore, the excavations of entrance facies can provide paleontological and archaeological remains. Interior facies can be defined as the sediments found more profound in the cave, beyond the reach of surface weathering, and that the interior cave dynamics deposited. In this environment, the clastic sediments are represented by clays, silts, and sands, in some cases described as accumulation by fluvial flows (Creer and Kopper, 1976; Bull, 1981; Bosch and White, 2004; Šroubek et al., 2007). The description of these facies is particularly interesting for studying the formation processes and hydrological dynamics of the endokarst (Iacovello and Martini, 2012; Arriolabengoa et al., 2015; Campaña et al., 2022; Kampolis et al., 2022). Despite this, these sediments have received much less attention than the entrance sediments.

Another point of view to classify sediments is given by Springer and Kite (1997), which separated between phreatic facies and vadose facies, with third residual facies, based on the study of the Cheat River (USA). Bosch and White (2004) presented a classification based on the clastic sediments' degree of sorting and particle size. This classification distinguished five sedimentary facies: diamicton, slackwater, channel, thalweg, and backswamp. This classification, modified by Herman et al. (2012), is explained in terms of the energy of the stream that transports the sediments inside the cave, albeit it is presented as a qualitative classification. Ford and Williams (2007) and White (2007) proposed three main groups: allochthonous, autochthonous, and chemical deposits; differentiating up to 23 principal origins for cave sediments, such as fluvial, aeolian, breakdown, calcite precipitation… etc. This classification is focused on the source of the deposit and has been widely used in the bibliography (Pérez-González et al., 1999; Goldberg and Sherwood, 2006; Campaña et al., 2017, among others).

The karst of the Sierra de Atapuerca hosts some of the most important spots for understanding human evolution in Europe during the Early and Middle Pleistocene (Carbonell et al., 2008; Rodríguez et al., 2011; Bermúdez de Castro et al., 2017; Martín-Francés et al., 2020; Rodríguez-Gómez et al., 2022). This karst is characterized by three sub-horizontal levels of cave developed at 1012, 1001 and 985 m elevation, whose formation is related to the evolution of the middle Arlanzon River (Ortega et al., 2013; Benito-Calvo et al., 2017) (Fig. 1). During the late 19th century, a railway trench cut through the south of the Sierra de Atapuerca, revealing numerous infilled caves and karst features of the intermediate level of the karst. These caves include the archaeological sites of Gran Dolina cave, Galería Complex and Sima del Elefante cave.

In the caves exposed in the railway cutting, interior facies sediments have been found in the bottom of Gran Dolina cave and Galería Complex (Pérez-González et al., 1995, 2001), meanwhile, no interior facies has been described in Sima del Elefante cave (Rosas et al., 2006). These sediments have distinct differences from the entrance facies sediments found in these fills, such as color, dominated by yellows and light browns, and texture, mainly sand, silt, and clay. Whereas the interior facies of Gran Dolina cave have been studied (Campaña et al., 2022), the Galería Complex's cave interior sediments lack a detailed description and interpretation, even though it has the longest stratigraphic section. The study of these facies can help to understand the evolution of the karst system and between Gran Dolina cave and Galería Complex, whose evolution should be related since geophysical studies indicate a connection between them (Bermejo et al., 2017).

The interior sediments in the Galería Complex cave also have an issue with its chronology since TT-OSL and ESR/U-series have dated it at an approximate age of 300–400 ka (Demuro et al., 2014). This age disagrees with the polarity reversal identified in the central part of the sediment succession that has been attributed to the Matuyama-Bruhnes boundary (Pérez-González et al., 2001) (Fig. 2). Therefore, the interpretation of the geochronology data is a challenge since the overlying units have concordant ages with the paleomagnetism boundary and the lack of knowledge about the formation processes of this deposit does not allow us to understand the young ages.

The aim of this work is to understand the cave dynamics and the hydrological regime of the middle level of the Sierra de Atapuerca karst system from the cave interior facies of the Galeria Complex, to interpret their depositional environment, the influence of surface-subsurface interactions in the sedimentation, and to compare these sediments with other karst infills. The study also seeks to understand the post-depositional processes of these deposits that may explain their dating problems. A multiproxy research approach has been done using sedimentological and mineralogical studies, to do a facies analysis of the sedimentological record. Thus, this study provides a detailed description of the stratigraphy and sedimentology of a section of >6 m thick and about 20 m long of sediments from cave interior facies.

2. Geologic context

The Galería Complex site is situated in the south of the Sierra de Atapuerca in north Spain (N42°21′05.29″; W3°30′39.20″; WGS84) (Fig. 1). The Sierra de Atapuerca is an NNW-SSE trending anticlinal ridge belonging to the most north-western outcrop of the Iberian Chain and is situated in the NE Neogene Duero Basin (Benito-Calvo and Pérez-González, 2015). This anticlinal ridge is composed of Late Cretaceous limestones and dolostones, and was folded during the Oligocene-Early Miocene. This deformation caused the deposit of syn-orogenic conglomerates, sandstones, and mudstones.

2.1. Geomorphology

In the Late Miocene-Pliocene, the Duero Basin was opened to the Atlantic Ocean, ending the endorheic phase and starting a phase of fluvial incision. During the Quaternary, the main fluvial systems around the Sierra de Atapuerca are the Arlanzón River and its tributaries, the Vena and Pico rivers (Fig. 1). The studies of the evolution of these rivers identified a terrace sequence of 14 levels, named from oldest (T1) to youngest (T14) (Zazo et al., 1987; Benito-Calvo et al., 2008; Benito-Calvo and Pérez-González, 2015) that was dated from the Early Pleistocene to the Holocene (Benito-Calvo et al., 2008; Moreno et al., 2012; Benito-Calvo et al., 2018). Terraces T1 (+92–97 m) to T4 (+60–65 m) have been constrained to the Early Pleistocene (1.14 ± 0.13 Ma, and between 0.78 ± 0.12–0.93 ± 0.10 Ma, respectively), while T5 (+50–58 m, 0.70 ± 0.10–0.60 ± 0.11 Ma) to T11 (+12–14 m, 0.14 ± 0.02 Ma) and T12 (+10–11 m) to T13 (+5 m) have been correlated to the Middle and Late Pleistocene, respectively. Finally, T14 (+2–3 m) was tentatively attributed to the Holocene (Moreno et al., 2012; Benito-Calvo and Pérez-González, 2015). These chronologies indicate a possible relation of the terrace deposits with cold Marine Isotope Stages and have allowed reconstruction of the incision rate evolution of the main valley (Benito-Calvo et al., 2017; Benito-Calvo et al., 2018).

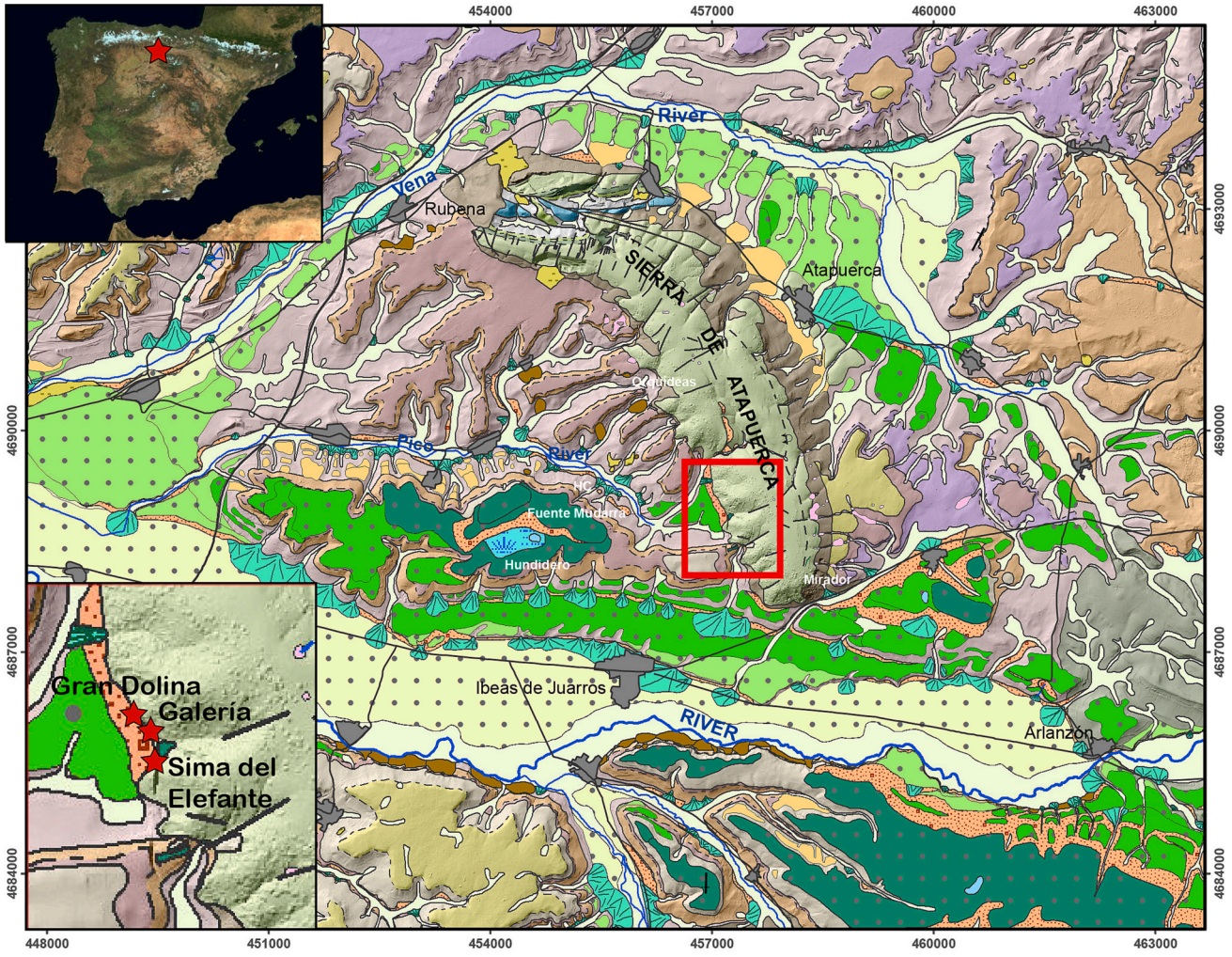

Legend

- Drainage network
- Floodplains and valleys beds
- Holocene fluvial terraces
- Upper Pleistocene fluvial terraces
- Middle Pleistocene fluvial terraces
- Lower Pleistocene fluvial terraces
- Cones
- Seasonal pools
- Semi-endoreic areas
- Alluvial-colluvial glacis
- Landslides
- Colluvial deposits
- Doline floors
- Dumps
- Roads
- Populations
- Archaeological sites
- Cross-section
- Limestones (Upper Miocene)
- Marls and limestones (Upper Miocene)
- Limestones with flint (Middle Miocene)
- Sands, silts and clays (Middle Miocene)
- Limestones (Lower Miocene)
- Marls, evaporites and clays (Lower Miocene)
- Conglomerates and clays (Oligocene-Lower Miocene)
- Limestones and dolostones (Upper Cretaceous)
- Limestones, marls and shales (Upper Cretaceous)
- Calcarenites, marls and limestones (Upper Cretaceous)
- Sands, gravels and clays (Lower Cretaceous)
- Limestones, sandstones and conglomerates (Lower Cretaceous)
- Dolostones and limestones (Jurassic)
- Conformity
- Unconformity
- Inferred overturned anticline
- Thrust

Fig. 1. General location and geological map of the Sierra de Atapuerca (after Benito-Calvo and Pérez-González, 2015).

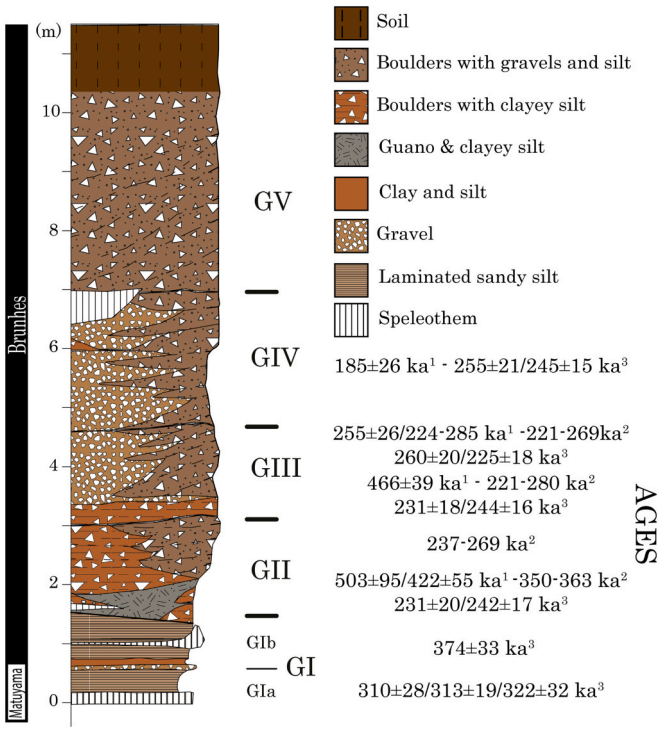

Fig. 2. Galería stratigraphic column (modified from Pérez-González et al., 2001 and Núñez-Lahuerta et al., 2022). Ages: 1- Berger et al., 2008; 2- Falguères et al., 2013; 3- Demuro et al., 2014.

2.2. Sierra de Atapuerca endokarst system

The multilevel endokarst system of the Sierra de Atapuerca was developed in the Early and Middle Pleistocene, and it was formed in the Late Cretaceous limestones and dolostones. This karst system consists of 4.7 km of explored passages (Martín-Merino et al., 1981), composed mainly of three levels of phreatic conduits, with some vadose trenches (Ortega, 2009; Ortega et al., 2013). These levels appear spatially and chronologically related to some of the Arlanzón fluvial terraces (Ortega et al., 2014, 2013; Benito-Calvo and Pérez-González, 2015; Parés et al., 2016; Benito-Calvo et al., 2017, 2018) (Figs. 3 and 4). The karst passages developed in a relatively short period corresponding to terrace aggradation, while the vadose entrenchments in the caves are related to longer incision phases of the Arlanzón River, as suggested by the relationship between the ESR dates of the terraces and the karst (Moreno et al., 2012; Benito-Calvo et al., 2018). Cave sediments are usually composed of interior facies made of quartzose sands and metamorphic gravels, located at the base and probably related to the Arlanzón inputs, and allochthonous sediments coming from the Sierra de Atapuerca upper slopes, derived from the weathering and transport of Upper Cretaceous carbonate bedrock or Duero basin Cenozoic sediments into the caves during vadose conditions (Pérez-González et al., 2001; Campaña et al., 2016, 2017). During the formation of the karst, the Arlanzón waters entered the galleries, passed through the interior of the karst, and left at springs in the Pico Valley headwaters (Ortega et al., 2013; Benito-Calvo et al., 2017) (Fig. 1).

The upper level developed in a position similar to the base levels associated with the fluvial terrace T2 (+82–86 m) (Ortega et al., 2013), which occurs at a similar elevation near the Sierra de Atapuerca (Benito-Calvo and Pérez-González, 2015; Benito-Calvo et al., 2018). This level is composed of Galería del Sílex, El Portalón, Salón del Coro, Galería de las Estatuas, and Galería de las Estatuas entrance (Fig. 4), having a total passage length of >600 m long, and ceilings at 1015–1022 m in altitude, some vertical chimneys reaching 1030 m in altitude (Ortega et al., 2018). The Salón del Coro, which has phreatic and vadose morphologies, is the most extensive cavity of the Sierra de Atapuerca karst and includes three distinct cave levels. The sediments at this level are mainly composed of clay and silt, except for the entrance areas (Ortega, 2009).

The middle level is a sinuous subhorizontal phreatic passage about 700 m long at about 1000–1005 m in altitude, associated with the period of stability represented by terrace T3 (+70–78 m) (Ortega et al., 2018) during the Early Pleistocene (Benito-Calvo et al., 2008; Moreno et al., 2012; Benito-Calvo et al., 2017). The vadose regime at this level, characterized by vadose incision and speleothem growths in the caves, was marked by an incision of the Arlanzón River between T3 and T4 (+60–65 m) (Ortega et al., 2013; Benito-Calvo et al., 2017). Part of this

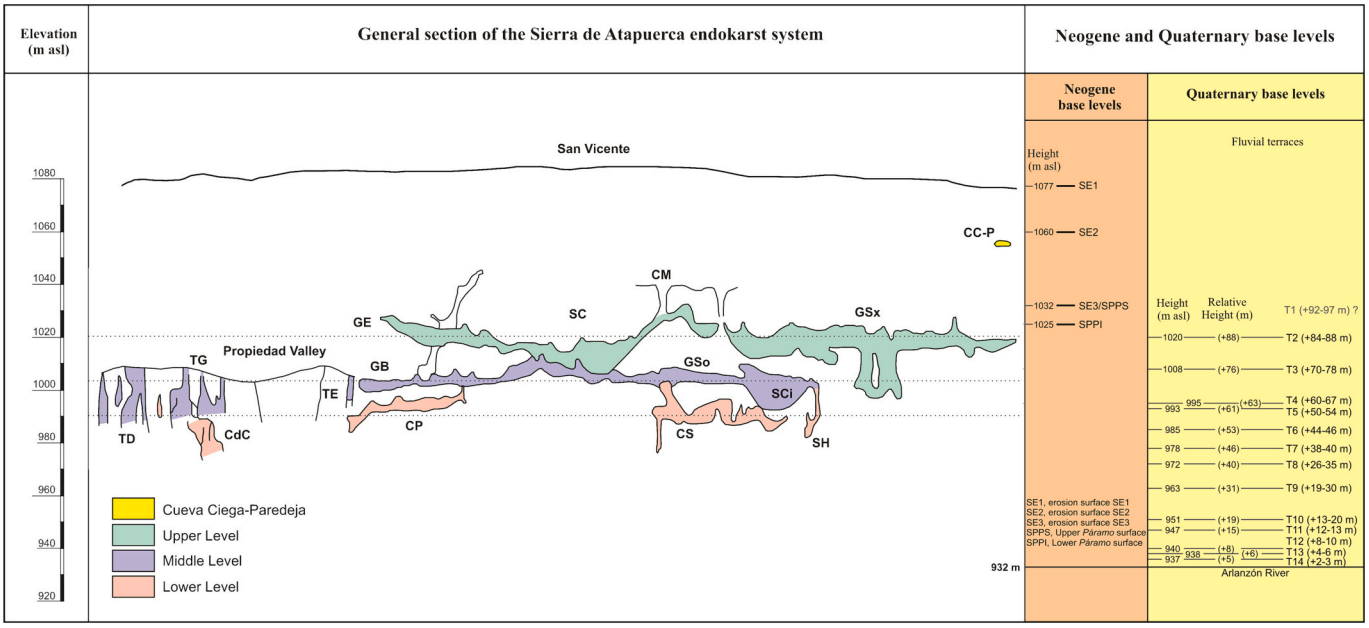

Fig. 3. General section of the Sierra de Atapuerca endokarst system and Neogene and Quaternary base levels. TD: Gran Dolina. TG: Galería Complex. CdC: Cueva del Compresor. TE: Sima del Elefante. GE: Galería de las Estatuas. GB: Galería Baja. CP: Cueva Peluda. SC: Salón del Coro. CM: Cueva Mayor. GSo: Galería del Silo. CS: Cueva del Silo. SCi: Sala de los Cíclopes. SH: Sima de los Huesos. GSx: Galería del Sílex.

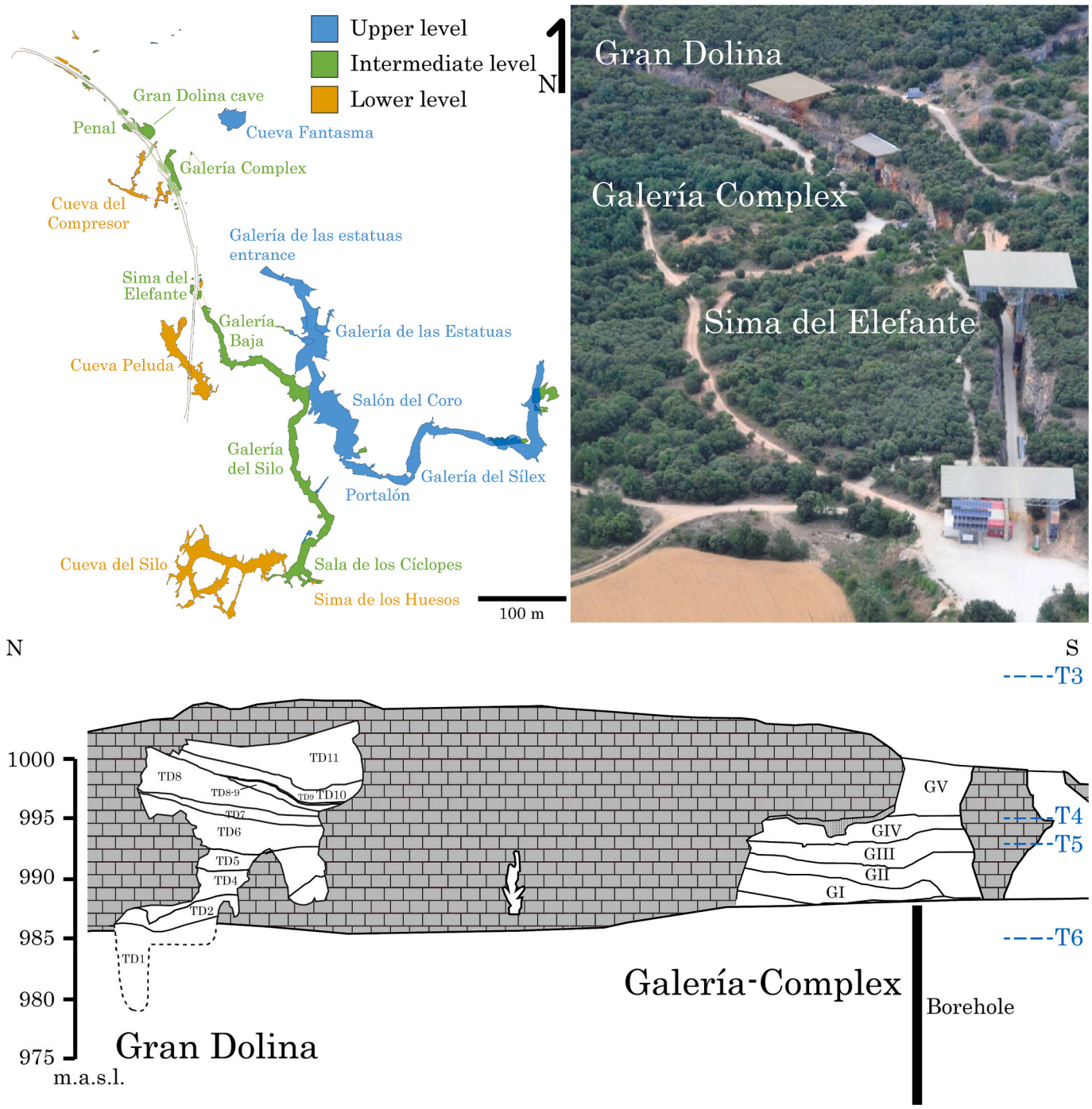

Fig. 4. Map of the Atapuerca multilevel cave system (modified from Ortega et al., 2013 and Ortega and Martín (in press)), aerial image of the Railway Trench with the situation of Gran Dolina, Galería Complex and Sima del Elefante, and schema of the Gran Dolina and Galería section with the Quaternary base levels indicated by terraces T3, T4, T5 and T6; and the location of the borehole. The underground karstic infills of the map of the Atapuerca multilevel cave system are pale green (Bermejo et al., 2020).

level was revealed by a railway cutting that cut the south of the Sierra de Atapuerca, showing numerous sedimentary fills with sediment up to the ceiling. Three important archaeological sites are located in this railway cutting: Sima del Elefante cave, Galería Complex cave, and Gran Dolina cave (Ortega et al., 2018), which preserve important archaeological and paleontological remains (Rodríguez et al., 2011). In addition, this level includes the passages formed by Sala de Los Cíclopes, Galería del Silo, and Galería Baja and its continuity up to the entrance of Sima del Elefante cave entrance (Fig. 4), as well as other recently discovered sediment-filled galleries (Bermejo et al., 2017; Bermejo, 2021).

The lower cave level has been correlated to the T4 (+60–65 m)/T5 (+50–54 m) (Ortega et al., 2013). Their ceilings are situated at 990 m a.s.l with vertical chimneys reaching 994 m in altitude (Ortega et al., 2018). This level is located further west than the upper and middle levels and is formed by Cueva del Silo, Cueva Peluda, Cueva del Compresor, and Sala del Caos (Fig. 4). Smaller in width than the caves on the other levels, and with less overall length, these conduits have a phreatic morphology (Ortega et al., 2014). The dating of some fluvial sediments from this level indicates re-sedimentation processes inside the karst, as ESR ages of 1.268 ± 0.133 Ma and 1.262 ± 0.108 Ma were obtained

from these sediments, while the formation of the lower cave level has average ESR ages of about 0.85 Ma from the dating of the terraces T4 and T5 (Moreno et al., 2012; Benito-Calvo et al., 2017; Hernando-Alonso et al., 2022), therefore, these fluvial sediments must come from the upper levels of the karst. Of these caves, Compresor cave is situated a few meters from Galería Complex. In this cave, quarrying activities for the extraction of building stone were carried out during the XXth century.

A small karst sublevel has developed in the south of the lower level. To this sub-level belongs Sima de Los Huesos and the lowest area of Silo cave, which has ceilings below 985 m.a.s.l (Ortega, 2009) (Figs. 3 and 4).

2.3. Gran Dolina site

Gran Dolina site, located <50 m north-west of Galería Complex (Figs. 4 and 5), is a 25 m thick sediment-infilled cave separated into 12 main lithostratigraphic units, with a total of 19 sedimentary facies identified so far (Campaña et al., 2017). The cave shows a key-hole morphology and, in spite of the name, it consists of a conduit sectioned by the slope. The 12 lithostratigraphic units were named TD1–TD11 (includes TD8–9 unit, defined later) from bottom to top (Gil et al., 1987; Parés and Pérez-González, 1999), of which TD1 and TD2 were defined as cave interior facies, whereas TD3 to TD11 were defined as cave entrance facies (Campaña et al., 2017, 2022).

TD1 and TD2 have been separated into five sub-units and 13 layers (Table 1), within which eight sedimentary facies have been described based on particle size and sedimentary features (Table 2). TD1 deposits are mainly characterized by the alternating millimetric lamination of 10YR 6/4 light yellowish-brown silty sand and clayey silt, with cemented layers and speleothems (flowstones and stalagmites) (Fig. 5). TD2 deposits start with a breakdown of the cave's walls and ceiling, followed by alternating laminated 10YR 6/4 light yellowish-brown sand and strong yellowish-brown silty sand, to finish with a 40-cm thick speleothem. The chronology of these units has been estimated between ~1.30 Ma and ~0.9 Ma (Parés et al., 2018; Duval et al., 2022; Campaña et al., 2022). These units were formed in the early Pleistocene after the vadose incision of the cave and their sedimentary facies indicate that the cave experienced alternating phases of phreatic and vadose conditions (Campaña et al., 2022). Overall, this indicates that the cave had general epiphreatic conditions.

TD3, a clayey unit described by Gil et al. (1987), is not preserved in the current section at Gran Dolina, where TD2 is overlain by TD4. From TD4 to TD11, the cave was filled in by entrance facies, which means that they were formed by sediments entering the cave through a nearby entrance. Therefore, the TD4 unit represents the opening of the cave to the outside. The cave was filled until it was completely silted up by the TD11 unit. Entrance facies of TD4 through TD11 units are separated into sedimentary gravity flow (debris fall, debris flow, and mud flow) and fluvial facies (channel, floodplain, and decantation) (Campaña et al., 2017; Campaña, 2018). These units have a chronology between ~0.9 Ma and ~0.2 Ma (Falguères et al., 1999; Berger et al., 2008; Arnold et al., 2015; Moreno et al., 2015; Parés et al., 2018; Álvarez-Posada et al., 2018; Duval et al., 2018), with the Matuyama/Bruhnes paleomagnetism boundary identified in the top of the TD7 unit (Parés and Pérez-González, 1995). During the Early Pleistocene (TD4 – TD7 units), Gran Dolina acted as a stream sink, where occasional and rapid gravity sediment flows occurred. Stream facies show a migration from TD4 to TD5, where the channel developed close to the NW cavity wall, until TD6, where the stream channel formed in the middle of the cavity. In the Middle Pleistocene (TD8 – TD11 units), fluvial facies decreased drastically, and the sequence was dominated by gravity flow facies (Campaña et al., 2017; Campaña, 2018).

2.4. Galería Complex site

The Galería Complex site is separated into three zones: Covacha de Los Zarpazos to the north, Galería in the center, and Tres Simas in the south (Fig. 6). The Covacha de Los Zarpazos section has been excavated for about 15 m in a passage trending direction northeast until it turned to the south in the Galería section. This cavity is mainly filled by interior facies, with entrance facies at the top. Galería is the main sub-horizontal conduit of the site. It is filled to the top by interior and entrance sediments (Pérez-González et al., 1995; Demuro et al., 2014). Tres Simas consists of three vertical vadose shafts; the first (TN) is connected in their lower part with Galería, and the other two (TC-TS) are connected between them, but in this sector they are not connected with the rest of the Galería Complex (Bermejo et al., 2020). The stratigraphic sequence of the Galería Complex has 13 m of thickness in the current section. An additional 17 m was proved in a borehole immediately adjacent to the exposed section (Bermejo et al., 2020). Thus the cave has >30 m thick sediments. From the bottom to the top, the sedimentary fill has been separated into five lithostratigraphic units (Pérez-González et al., 1995) (Fig. 2). GI is formed by interior facies while GII – GV is entrance facies composed of fluvial facies and debris flow facies grading towards the north into laminated sandy clay-loam (Pérez-González et al., 1995; Ortega et al., 2014).

Unit GI is formed by layers of fine laminated sands, silts, and clays with colors ranging from light yellowish brown to red. Its structure is sub-horizontal, although there are many post-depositional deformations and faults due to sediment accommodation, as well as erosional processes and reworking of levels of the unit itself. Within this unit, a paleomagnetic reversal attributed to the Matuyama-Bruhnes boundary (Pérez-González et al., 2001) was described that separates the unit into two sub-units: GIa below the boundary and GIb above it (Demuro et al., 2014) (Fig. 2). GII is the first entrance deposit of Galería with a thickness of 1 m to 2.5 m in the southern section and resting above GI in angular discontinuity (Pérez-González et al., 1995; Demuro et al., 2014). It is a heterogeneous unit that begins with a layer of collapsed limestone blocks and contains white and black levels of organic origin, which have been interpreted as bat guano deposits (Pérez-González et al., 1995). Sand grains of GII has been dated by luminescence, obtaining chronologies between 0.503 ± 0.095 Ma (Berger et al., 2008) and 0.231 ± 0.02 Ma (Demuro et al., 2014). Several of the limestone clasts of this unit are altered on their surface with phosphate crusts due to the reaction with the acidic phosphate rich guano (Pérez-González et al., 1999; Demuro et al., 2014). GIII and GIV have a similar lithology characterized by gravel levels in the central zone of Galería and gravity deposits at the sides. GIII has OSL dating of 0.244 ± 0.016 Ma and 0.26 ± 0.02 Ma (Demuro et al., 2014) and ESR of between 0.221 and 0.285 Ma (Falguères et al., 2013), while GIV has a luminescence chronology of 0.185 ± 0.026 Ma (Berger et al., 2008) and 0.255 ± 0.021 Ma (Demuro et al., 2014). Finally, unit GV corresponds to sediments deposited at the vertical entrance in the southern zone of Galería (TN), which is formed by at least six gravity flows of gravels with intercalations of silt and clay levels (Pérez-González et al., 1995). The sedimentary fill of the Galería Complex ends with an edaphic level of *Terra Rossa*.

The continuation of the Galería Complex with the rest of the karst of the Sierra de Atapuerca is not well understood. However, geophysical surveys indicate that this site is connected to Gran Dolina through the upper part of Covacha de Los Zarpazos (Bermejo et al., 2017).

The archaeological record of the Galería Complex site is found in GII and GIII. In these units, about 12,000 mammal fossils and approximately 1800 lithic tools have been recovered (Ollé et al., 2013). Among these fossils, two human remains attributed to *Homo* sp. *aff. heidelbergensis* have been found (Arsuaga et al., 1999; Rosas and Bermúdez de Castro, 1999). The lithic industry has been identified as technological mode II (Ollé et al., 2013). The site has been interpreted as a supply area for carcasses of large herbivores that may have fallen through the vertical entrance to the south of Galería (Ollé et al., 2005), although this

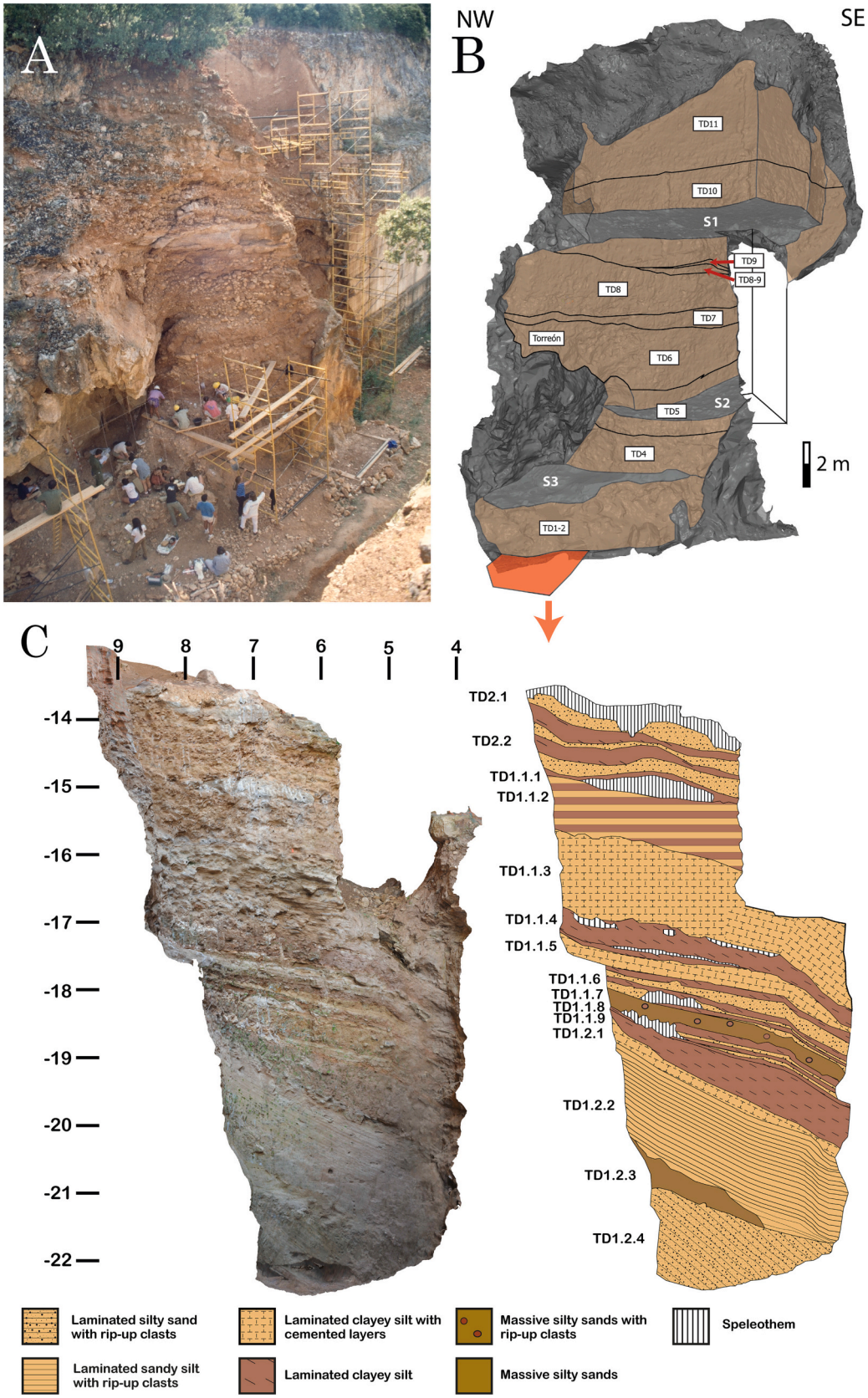

Fig. 5. (A) Gran Dolina site in 1994 (M. A. Martín). (B) 3D model of the Gran Dolina site in 2012. Brown areas indicate stratigraphic units. Grey areas are the wall and roof of the cave. The red area is the current situation of the TD1 and TD2 test pit. (C) Stratigraphic column of TD1 and TD2 (Campaña et al., 2022).

Table 1
Sedimentary description of the TD1 and TD2 sub-units and layers.

Sub-unit	Layer	Thick	Description
TD1.1	TD1.1.1	30	Speleothem
	TD1.1.2	70	Alternating of laminated 10YR 6/4 light yellowish-brown silt and clayey silt, partially cemented, with clay nodules. Speleothem growth is shown at the top.
	TD1.1.3	110	Millimetric lamination of 10YR 6/4 light yellowish-brown clayey silt with cemented sub-layers.
	TD1.1.4	45	Millimetric lamination of 5YR 4/4 reddish brown clayey silt with speleothem growth and limestone altered clast on the top.
	TD1.1.5	40	A cemented layer of millimetric lamination 10YR 6/4 light yellowish-brown clayey silt.
	TD1.1.6	50	Alternating 10YR 7/3 very pale brown silty sand and 5YR 4/4 reddish brown clayey silt, partially cemented and speleothem growth at the north.
	TD1.1.7	25	Massive 10YR 5/6 yellowish-brown silty sands with rip-up clasts of red clays, partially cemented.
	TD1.1.8	30	Alternating of 10YR 7/3 very pale brown silty sand and 5YR 4/4 reddish brown clayey silt, partially cemented at the north.
	TD1.1.9	50	Millimetric lamination of 5YR 4/4 reddish brown clayey silt.
TD1.2	TD1.2.1	20	Cemented millimetric lamination of 10YR 6/4 light yellowish-brown silty sand.
	TD1.2.2	180	Millimetric lamination of 10YR 6/4 light yellowish-brown silty sand.
	TD1.2.3	40	Massive 10YR 5/6 yellowish-brown silty sands.
	TD1.2.4	130	Millimetric lamination of 10YR 4/6 dark yellowish-brown silty sand and 5YR 4/4 reddish brown clayed silt.
TD2.1		40	Speleothem
TD2.2		100	Alternating of laminated 10YR 6/4 light yellowish-brown sand and strong yellowish-brown silty sand, partially cemented, with clay nodules.
TD2.3		100	One meter diameter limestone clasts from the ceiling and cave walls.

Table 2
Concise description of the sedimentary facies observed in TD1 and TD2 units (Campaña et al., 2022).

Facies		Sedimentary process	Description
A	A1	High-energy hydric flow	Millimetric laminated silty sand with rip-up clasts.
	A2	Medium-energy hydric flow	Millimetric laminated sandy silt with rip-up clasts.
	A3	Medium-energy hydric flow	Millimetric laminated clayey silt with cemented layers.
B		Low-energy hydric flow	Millimetric laminated clayed silt.
C	C1	High-energy hydric flow	Massive silty sands with rip-up clasts.
	C2	Parallel accretion	Massive silty sands.
D		Speleothem	Speleothem growth.
E		Breakdown	Large and angular boulders broke off from the ceiling and walls of the cave.

interpretation has been recently disputed (Santonja and Pérez-González, 2018, 2021).

3. Materials and methods

3.1. Sedimentological studies

The study and classification of the different facies and sedimentary environments of the Galería Complex required a detailed description of the available stratigraphic excavation profiles. The color of the layers has been described using the MUNSELL soil color chart. Fieldwork has been combined with laboratory analyses to describe the mineralogy and texture of the sediments, and five samples of sediment were taken from non-cemented layers in the stratigraphic section to make particle size, mineralogical and chemical analyses. Some of the layers of GI are composed of millimetric laminations that could not be distinguished during bulk sampling. Therefore, particle size analyses are the result of both kinds of laminates, a darker laminate and a lighter laminate. In these cases, a representative amount of samples was taken to assure to take both of them. Lateral variations are not a factor in this sampling because the layers are very homogenous laterally.

Particle size sieving and laser diffraction techniques have been used. For sieving techniques, φ size sieves ranging from −3φ to 4φ were used (Geology Laboratory, CENIEH). Larger sizes have not been analyzed because a large amount of sample would have been required to obtain a representative analysis. The particle size of the silt and clay fractions was measured using a Beckman Coulter LS13 320 laser diffraction particle size analyzer. Particle size has been classified following Blott and Pye (2012).

The survey of the stratigraphic profiles and facies maps of the sections was performed using total stations and photogrammetry (Digital Mapping and 3D Analysis Laboratory, CENIEH), which have served to obtain a 3D model of textures with an RGB image of Galería. Thus, ortho-images of GI were extracted from the 3D model to study the stratigraphic section, which were processed to balance the color and eliminate overprinted scaffolds. Due to the part of the section being covered by the scaffolds, old photographs were needed to complete the stratigraphic section.

AutoDesk AutoCAD 2020 was used to measure the section's deformation and faults.

3.2. Mineralogical and chemical analyses

The mineralogical and chemical composition of the bulk samples were obtained by combining two techniques at the Archaeometry Laboratory of the CENIEH, Spain. The mineralogical phase composition was determined by bulk mineralogy powder X-ray diffractogram (XRD) using a PANalytical X'Pert PRO instrument equipped with a Cu target and a secondary monochromator. The operating conditions for XRD were 45 kV/40 mA in a continuous scan mode performed in the range of 2θ from 3° to 70° with an increment of 0.02°. A semiquantitative analysis was carried out according to the Chung method (Chung, 1975) using High Score Plus software based on the Reference Intensity Ratios (RIR) of the existing phases.

Chemical compositions of the major elements were obtained by wavelength dispersive X-ray fluorescence method (XRF) using a PANalytical Axios instrument. For each sample, 0.5 g of bulk grounded material was homogeneously mixed with 5 g of 66:34 mixture of $Li_2B_4O_7$ and $LiBO_2$ flux with LiBr as bead releasing agent. The mixture was then fused to a glass bead in a Pt-Au crucible with a PANalytical Perl'X3 automatic fusion machine. The following elements were measured: SiO_2, Al_2O_3, Fe_2O_3 total, MnO, MgO, CaO, Na_2O, K_2O, TiO_2, P_2O_5, and SO_3. Loss on ignition (LOI) was calculated too.

4. Detailed stratigraphy and sedimentology of Galería Complex

4.1. Stratigraphy and facies of GI

GI is separated into two sub-units, GIa and GIb, by chronostratigraphic criteria, as the paleomagnetism boundary Matuyama-Bruhnes indicates the separation between the two sub-units, GIa is situated under this boundary, and GIb lies above it (Demuro et al., 2014). Each sub-unit has been separated into six layers following lithostratigraphic criteria; a concise description of each layer can be found in Table 3.

4.1.1. Particle size analyses

All the layers show a dominance of silt and clay components and very fine sand size (Fig. 7). The samples are named according to the

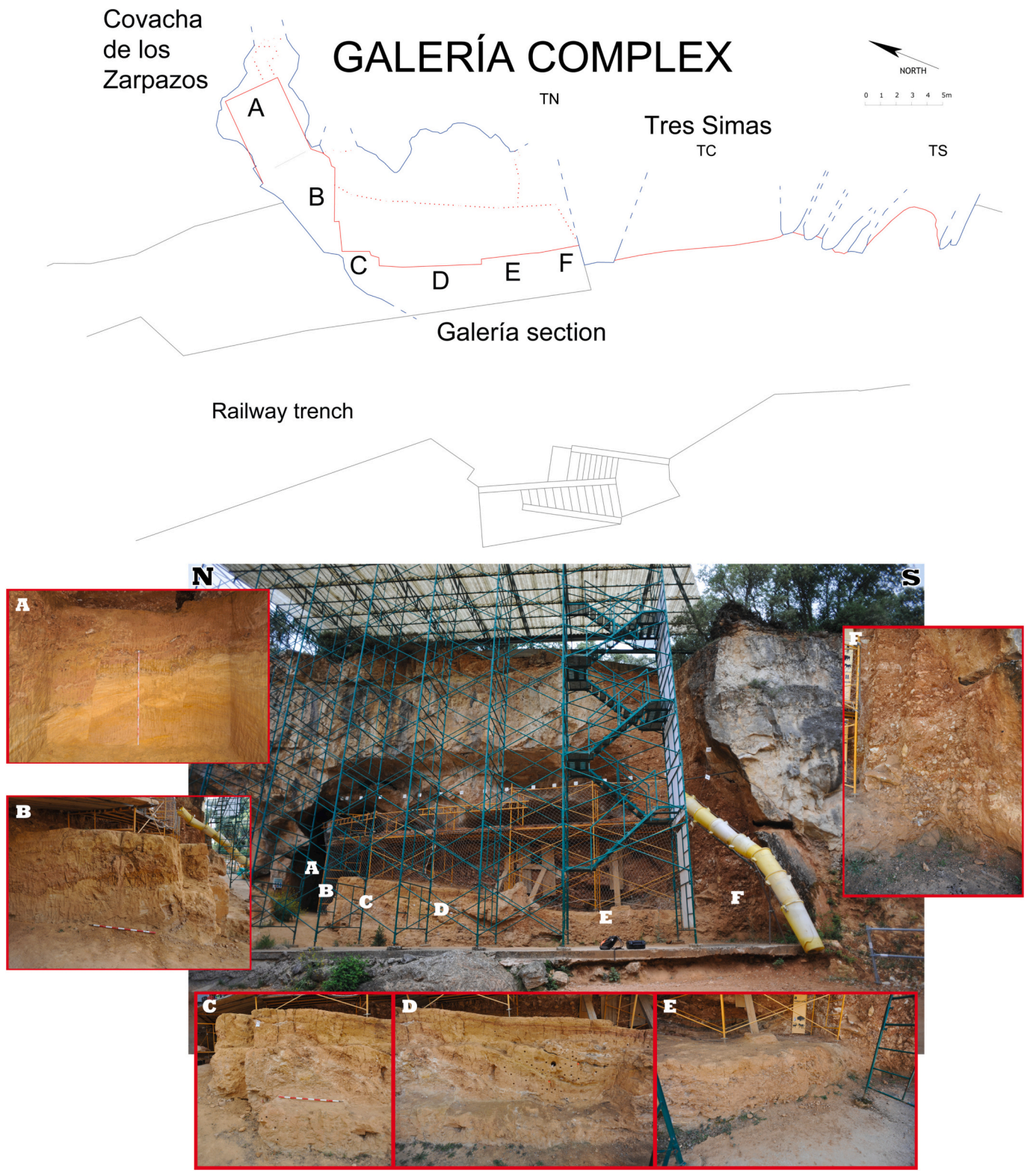

Fig. 6. Galería Complex with the situation of the GI areas. A and B images are from Covacha de Los Zarpazos area in 2010. C, D and E images are from the Galería area. F is the sinkhole situated in the south of Galería Complex.

sedimentological layer in which they were taken (Table 3). According to the particle size, the sedimentary layers can be divided into silt-clay layers (a.1, a.2, a.4) and sandy silt layers (a.3, a.5). Inside the silt-clay group, a.2 shows coarser sand distribution than the rest of layers that is due to the sands layers that this layer has. The sandy silt group shows a clear difference between the two layers, having coarser sand distribution a.3 than a.5 (Fig. 7).

4.1.2. *Mineralogy analyses*

The mineralogy of GI is very homogeneous. It is composed of quartz and phyllosilicate as the main minerals, with feldspar and phosphate as traces (Table 4). This mineralogy is according to the elemental results

Table 3
Sedimentary description of the GI layers.

Sub-unit	Layer	Thick	Description
GIa	1	25	10YR 6/4 light yellowish-brown clayed silt with cemented silt.
	2	60	Millimetric lamination of 5YR 4/4 reddish brown silty clay with layers of fine sand. About 10–15 cm thick speleothem and gravels layers are observed to the south.
	3	30	Massive 10YR 5/6 yellowish-brown sandy silt.
	4	20	10YR 5/3 brown clayed silt with cemented silt.
	5	310	Fine laminated 10YR 7/3 very pale brown to 10YR 5/4 yellowish brown sand, silt, and clays.
	6	>250	Alternating 5YR 4/4 reddish brown silty clay, 10YR 5/6 yellowish-brown sandy silt, 2.5Y 5/4 light olive brown sand, and calcilutite.
GIb	1	25	Centimetric lamination of clay, silt, and sand.
	2	60	10YR 5/4 yellowish-brown silt.
	3	100	10YR 6/4 light yellowish-brown silt with rip-up clasts of silt and clay.
	4	70	Speleothem
	5	15	10YR 6/6 brownish-yellow silt with limestone gravels and rip-up clasts of silt and clay.
	6	30	10YR 6/6 brownish-yellow silt with rip-up clasts of silt and clay. At the bottom, a 2–4 cm thick layer with coarse sand and fine gravel is observed.

(Table 5). The layers a.1 and a.5 have lesser values of Al and K than the rest of the layers, which can be correlated with the amount of phyllosilicate. These layers also show less iron oxide, suggesting that it could be related to the phyllosilicate.

Two kinds of phosphate have been found: hydroxylapatite and crandallite, which are traces according to the elemental results (Table 4). Noteworthy, the layer with apatite has more P and Ca than the other layers, and no calcite is identified (Table 4). All the Ca found can be explained by phosphate minerals, while the LOI values can be due to water, carbonate, and hydroxyl ions in the structure of phosphate minerals.

Although rutile is not identified in the XRD analyses, the results of chemical analyses, with about 1 % of Ti (Table 5), indicate the existence of this mineral in the sediment, as is described in Gran Dolina and Galería sediments (Aleixandre and Pérez-González, 1999; Campaña et al., 2017, 2022).

4.1.3. Detailed stratigraphy of GI

The first layer observed in the section is GIa.6 in the Covacha de Los Zarpazos (Figs. 8, 9, 10, 11 and 12), which is formed by cycles of sandy silt, laminated silty clay, medium and fine massive sand and cemented lutites (Fig. 10). At least four cycles are observed in the section, although there may be more in-depth. All these layers show soft-sediment deformation structures, with low-angle folds and fractures, which caused the discontinuity of some levels and the dip to the north. GIa.6 ends with a cemented lutite, suggesting that this lithology represents the end of the cycle.

GIa.5 overlies GIa.6 in angular discordance. This layer consists of >3 m of millimeter-thick laminated yellowish and reddish sandy silts with some cross-lamination and cut-and-fill structures (Fig. 10). The laminae are composed of medium sands, silts, and clays and vary in thickness from less than a millimeter to several centimeters. Color is related to particle size, with clay being redder and sand being yellower. At about 1 m above the surface, there is a change between reddish laminas dominated by clayey sediments and yellowish laminas dominated by sandy sediments (Fig. 10). Speleothem growth is observed in the Galeria section (Fig. 12).

GIa.4 is a massive layer of clayey silt, about 15 cm thick, which is concordant with GIa.5. This layer is locally deposited only in the Covacha de Los Zarpazos area, and is not found in the Galería area. On top of this layer is GIa.3, which is a sandy silt layer with no clear lamination and a thickness of about 50 cm. This layer has a plastic behavior and shows slight folds, thinning and thickening in section caused by post-depositional processes (Fig. 11). Overlying this layer is GIa.2.

GIa.2 consists mainly of millimeter thick layers of silty clay with some sand layers of about 1 cm. These sand layers are of a yellowish color. Laterally, this layer shows great complexity to the south (Fig. 12), where at least two speleothem growths can be observed in the outcrop section, although there may be more under the current section; and some lenticular-shape levels of angular carbonate rock gravels. These last levels consist of grain-supported gravels composed of centimeter size clasts that indicate at least three different events.

GIa.1 is similar to GIa.4. It is about 15 cm thick of massive clayey silt deposited in a concordance boundary with the underlying layers. GIa.1 is observed with certainty only in the Covacha de los Zarpazos, being certainly eroded in the rest of the surface. It is also found in the Galería section, which dips to the south and has been eroded (Fig. 12), and in the upper part of the Covacha de los Zarpazos, where it appears as a slightly folded horizontal level cut by faults (Figs. 9 and 10). Although these two layers have been related because of their spatial position above GIa.2, they could be different, diachronous layers. Paleomagnetic analyses in the upper part of the Covacha de Los Zarpazos could provide more data on this issue.

GIb is divided into six layers. The first two layers, GIb.6 and GIb.5, are observed only in the southern part of the section (Fig. 12) and are very similar, described as brownish-yellow silt with rip-up clasts. Overlying these two layers is a stalagmite (Fig. 12). This is the thickest speleothem growth seen in GI, and it is in the same vertical position as the speleothem described in GIa.2, suggesting a drop area.

GIb.3 is an irregular layer that varies in thickness from 20 cm to 2 m and rests discordantly with the lower layers. GIb.3 is formed by yellowish-brown silt with rip-up clasts of silt and clay. Some of these rip-up clasts can reach up to 30 cm in diameter, in Covacha de los Zarpazos. GIb.2 is found in concordance with GIb.3 and they are very similar. GIb.2 layer is a massive silt deposit without rip-up clasts that represents the last deposit of GI in much of the Galería Complex (Fig. 8).

The sedimentation process ended with GIb.1, which consists of a 25 cm thick layer of centimeter-sized clay, silt, and sand laminations. The laminations vary in color from red to yellow depending on the particle size of each layer. Each layer appears to have similar characteristics to the previous GI layers, indicating reworking processes. The thickness of the layer increases to the south and wedges to the north before reaching the Covacha de los Zarpazos. In addition, this layer has a slight dip to the south.

4.1.4. Facies of GI

The study of the stratigraphic section of GI and Covacha de Los Zarpazos has allowed a new sedimentary facies classification to be made for the site. This classification follows sedimentologic criteria as field observation, particle size analyses, and previous cave sediment classifications (Miall, 1978; Ford and Williams, 2007; White, 2007; Pérez-González et al., 2001; Campaña et al., 2017; Campaña et al., 2022).

According to the classifications of Kukla and Lozek (1958) and Creer and Kopper (1976), these facies are classified as interior facies. They consist of sand, silt, and clay (Fig. 7) with a notable absence of larger sedimentary particles. It is possible that this absence of coarse sediments in the Galería complex is because of the distance from the sediment's entrance into the karst. This distance could have sieved out the coarse sediments, leaving only finer ones available, similar to what was observed in the Gran Dolina cave nearby (Campaña et al., 2022). This sieving process might have prevented the deposition of gravel, even during high-energy stream flows in the karst.

For easy comparison, the facies have been named for their similarity with the interior facies described in the nearby Gran Dolina site (Campaña et al., 2022) (Table 6).

Facies A: Millimetric laminated 10YR 7/3 very pale brown to 10YR

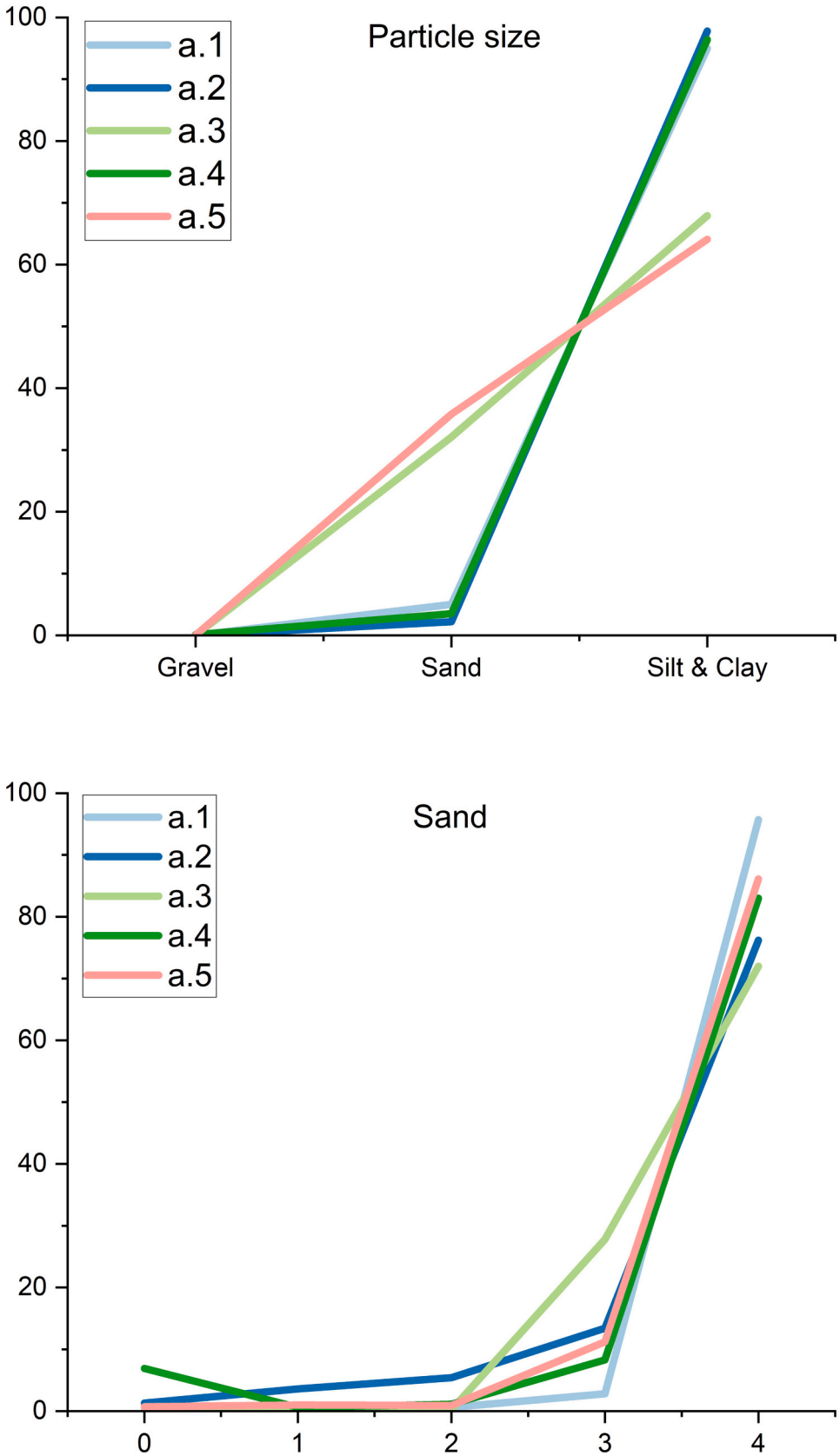

Fig. 7. Particle size distribution of the stratigraphic layers of GIa. Axis of abscissa – Phi size.

Table 4
Mineralogy of the non-cemented layers of GI using XRD. +++ major phase > 30 %, ++ minor phase 30–10 %, + traces < 10 %.

Layer	Quartz	Feldspar	Phyllosilicate	Apatite	Crandallite
GIa.1	+++	+	+		+
GIa.2	+++	+	+++		+
GIa.3	+++	+	++		+
GIa.4	+++	+	++	+	
GIa.5	+++	+	+		+

5/4 yellowish brown sandy silt with some millimetric sand layers composed of about 35 % of fine and very fine sand and about 65 % of silt and clay (Fig. 7). The lamination is inclined to adapt to the inherited morphologies. However, post-depositional processes can have modified the original deposit. It shows planar and cross-lamination with numerous cuts and fills in the section (Fig. 13A). The facies corresponds to Fl in Miall's classification (Miall, 1978). The boundaries at the base and top are sharp. Its mineralogy is mainly quartz, with traces of feldspars and phyllosilicates. Locally, there are areas with a higher predominance of clays. This facies is observed in GIa.5.

Facies A is similar to different cave facies described in the bibliography such as the facies A in the Gran Dolina site (Campaña et al., 2022), the cross-bedded coarse to find sands of the Galería de las Arenas (Hernando-Alonso et al., 2022), the slackwater facies of Lower Cerovačka Cave (Kurečić et al., 2021), or the laminated to massive sand (Sl/Sm) and Cut-and-fill sediments (Sc) of Sirijordgrotta (Norway) (Valen et al., 1997), among others. This kind of facies is relatively common in cave environments where laminated sand deposits have been described and interpreted as the result of a fluvial flow (Springer and Kite, 1997; Bosch and White, 2004; Laureano et al., 2016; Kurečić et al., 2021). This

Table 5
Chemical analysis of the non-cemented layers of GI using XRF. The results are expressed as oxides weight %.

Layer	SiO2	Al2O3	Fe2O3t	MnO	MgO	CaO	Na2O	K2O	TiO2	P2O5	SO3	LOI
GIa.1	77.26	9.32	3.24	0.02	0.46	1.14	0.13	1.90	1.12	1.91	bld	3.51
GIa.2	61.26	17.64	5.77	0.02	1.13	1.41	0.21	3.60	1.18	1.75	bld	6.02
GIa.3	71.91	12.52	4.19	0.03	0.67	1.18	0.13	2.09	0.97	1.49	bld	4.82
GIa.4	63.10	12.62	4.83	0.02	0.75	5.29	0.18	2.57	1.13	3.84	bld	5.68
GIa.5	82.25	7.58	2.40	bld	0.37	0.75	0.10	1.69	1.04	1.21	bld	2.60

Fig. 8. GI stratigraphic section from Covacha de Los Zarpazos to Galería area. The composition is formed by orthoimages made by photogrammetry (see Materials and methods).

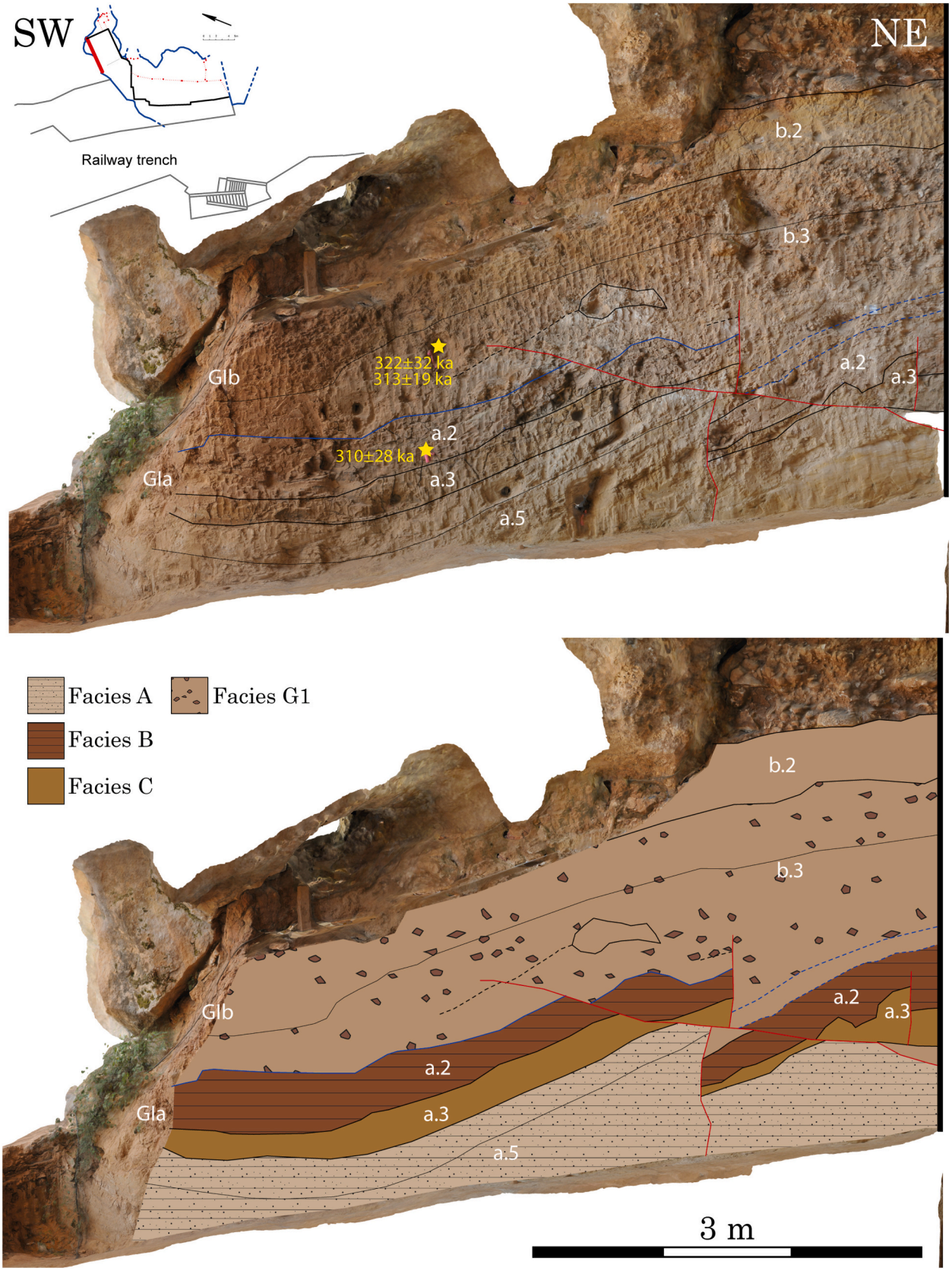

Fig. 9. NW stratigraphic section in Covacha de Los Zarpazos área. The composition is formed by orthoimages made by photogrammetry (see Materials and methods). SG TT-OSL dating marking by yellow stars (Demuro et al., 2014).

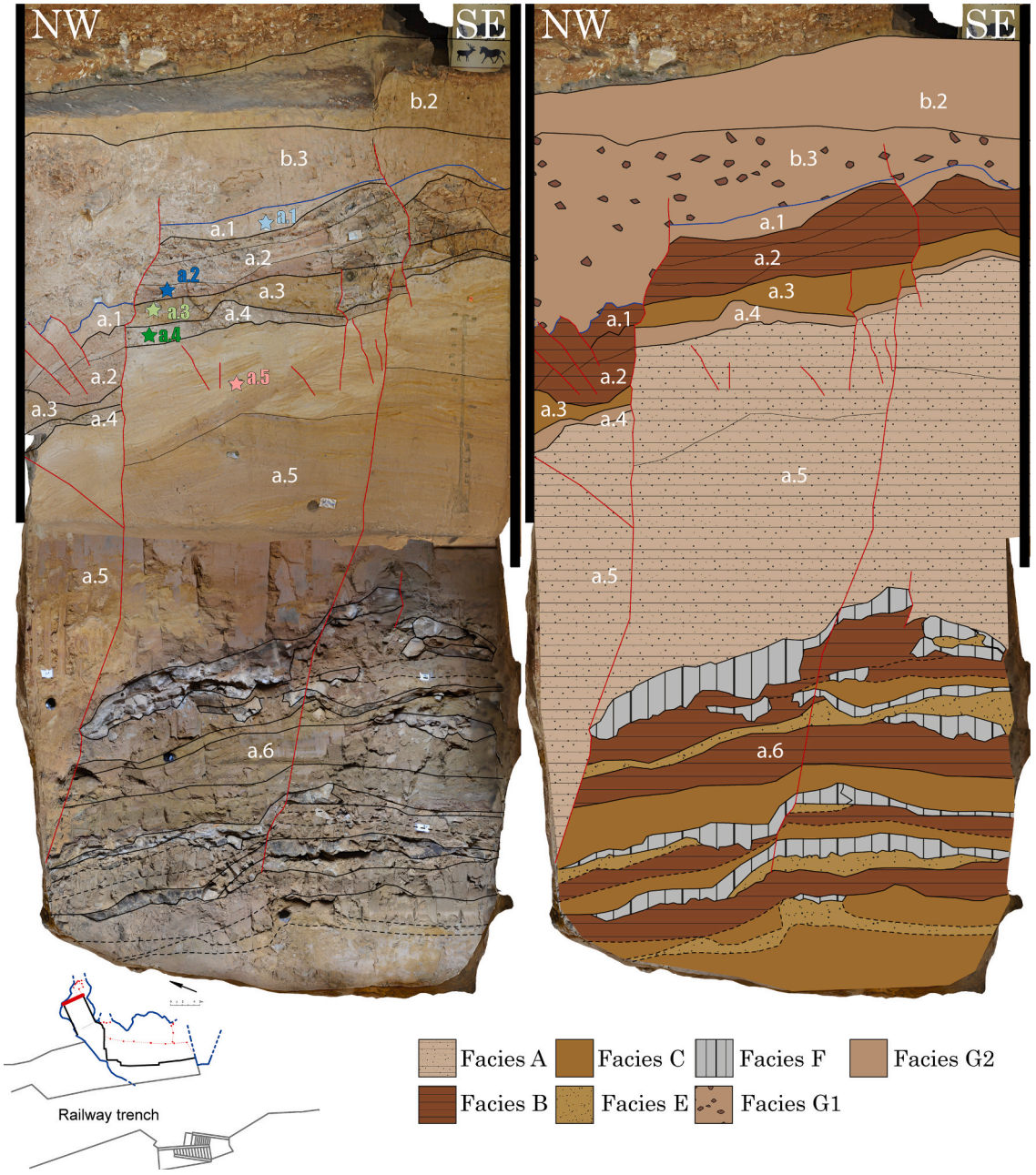

Fig. 10. NE stratigraphic section in Covacha de Los Zarpazos área. The composition is formed by orthoimages made by photogrammetry (see Materials and methods). The samples for particle size analysis and composition analysis are indicated by stars with the same colors as in Fig. 5.

kind of facies have been associated to different hydrological regimes, including high-energy environments in vadose conditions (Valen et al., 1997), and medium-energy environments in epiphreatic conditions (Springer and Kite, 1997; Bosch and White, 2004). Based on the lack of gravels, a relatively medium-energy low-gradient stream can be associated with facies A.

Facies B: Millimetric lamination of 5YR 4/4 reddish brown silty clay that is composed of >90 % of silt and clay (Fig. 7), with the main mineralogy of quartz and phyllosilicates and intercalations of fine sand layers (Fig. 13B). These fine sand layers are pale reddish-yellow and can have a few centimeters thick. No vertical particle size variation is observed in these facies. It can be also considered as Fl in Miall's classification (Miall, 1978), as facies A, but with less energy. This facies presents a sharp base and top boundaries. The lamination is tabular, mainly horizontal, with slight folds. This facies is observed in GIa.2, GIa.5, and GIa.6.

The facies B is similar to the red mud facies described in many caves (Bull, 1981; Springer and Kite, 1997; Auler et al., 2009; Martini, 2011; Iacovello and Martini, 2012; Laureano et al., 2016; Kaufmann et al., 2020; Martín-Perea et al., 2022), including the near Gran Dolina site (Facies B in Campaña et al., 2022). These deposits' particle size and lamination have been usually explained as the result of sequential flooding events that can build up very fine-scale layering (Bull, 1981; Fornós et al., 2009; Herman et al., 2012), although aeolian sources have been also postulated to similar facies such as Wet Cave Unit A (Macken et al., 2013) and Robertson Cave Lower Unit (Forbes and Bestland, 2007), both from Naracoorte caves. The deposits of this cave were deposited in arid conditions and showed a high concentration of water-soluble minerals (Forbes and Bestland, 2007), which are not the case for the Galeria Complex's facies B (Table 4); in addition, the millimetric lamination indicates that water was a significant agent of sediment transport as suspended load, as other authors are indicated to similar

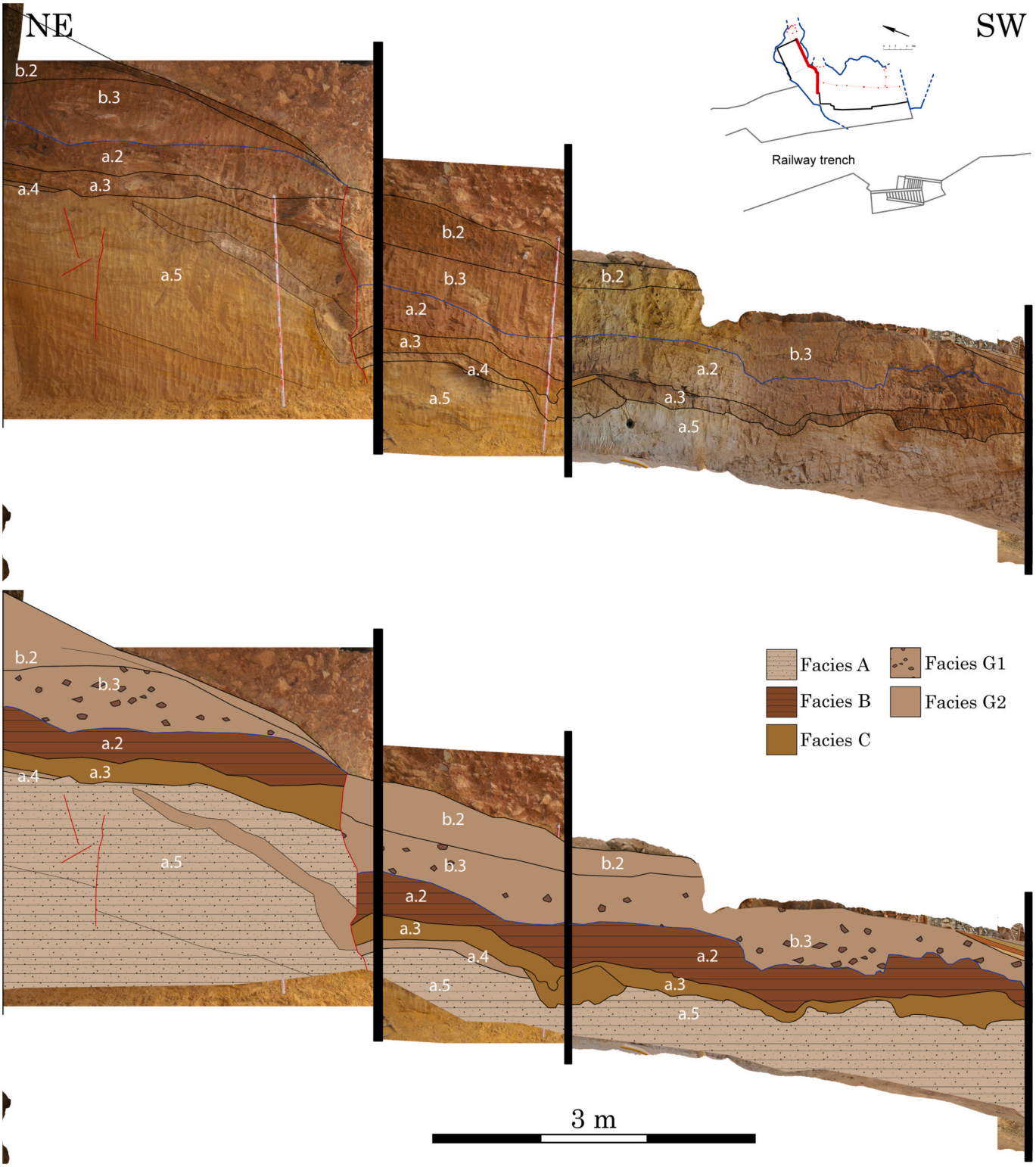

Fig. 11. SE stratigraphic section in Covacha de Los Zarpazos área. The composition is formed by orthoimages made by photogrammetry (see Materials and methods).

deposits (Martini, 2011; Iacovello and Martini, 2012). In this sense, facies B would indicate a hydrological regime with lesser energy than facies A, in which suspended sediments have time to settle out, but the sand layers of facies B can be interpreted as flooding events with enough energy to drag the sand, therefore, in these events, the facies B flow may have a similar energy to the facies A. In this sense, facies B is interpreted as the deposit of a medium to low-energy fluvial system with occasional moments of higher energy indicates by the sand layers, suggesting an environment with fluctuation in the flow.

Facies C: Massive 10YR 5/6 yellowish-brown sandy silts composed of about 30 % of fine and very fine sand and about 70 % of silt and clay (Fig. 7). It is observed in GIa.3 and GIa.6. Rarely, small sand and clay laminates can be appreciated, especially in GIa.6 deposits. This facies is Fm in Miall's classification (Miall, 1978). The top and base boundaries

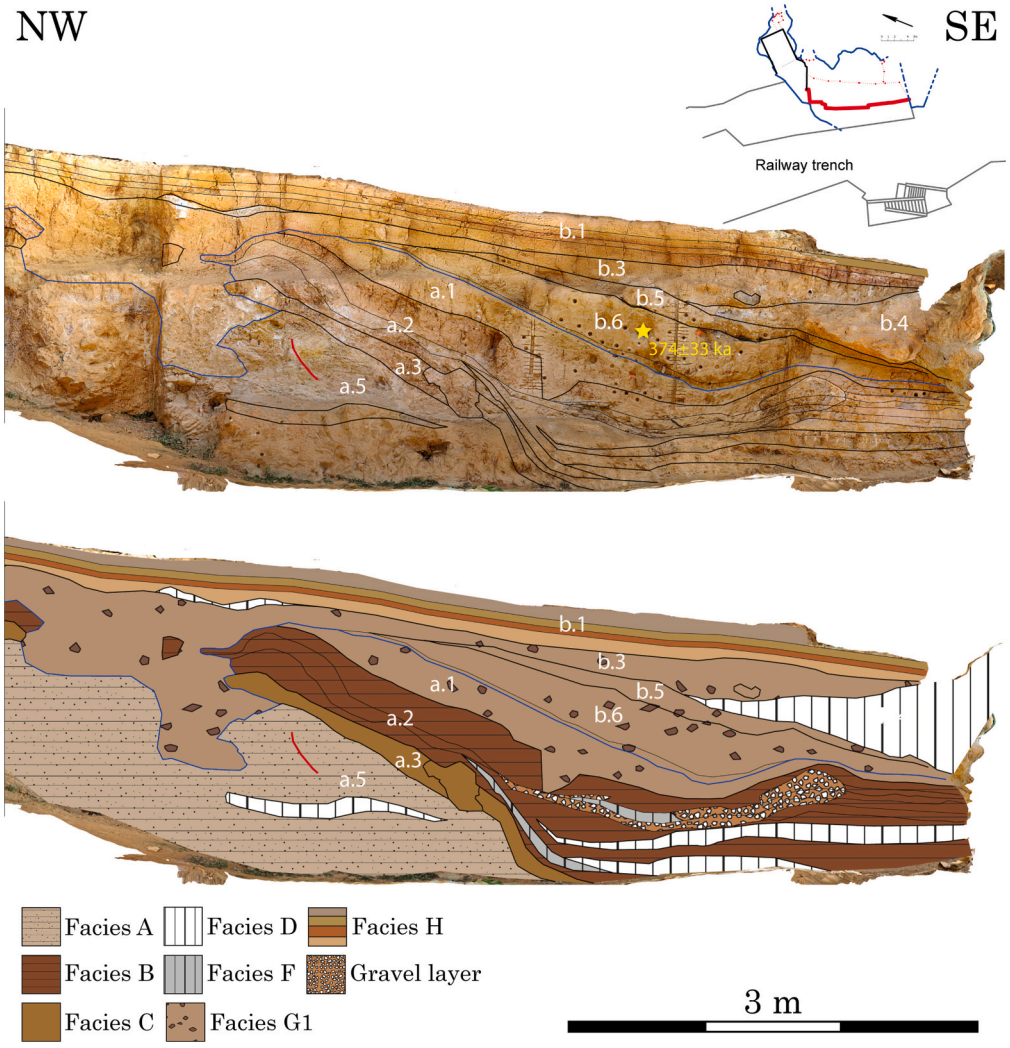

Fig. 12. NE stratigraphic section in Galería area. The composition is formed by orthoimages made by photogrammetry (see Materials and methods). SG TT-OSL dating marking by yellow star (Demuro et al., 2014).

Table 6
Concise description of the sedimentary facies observed in the GI unit.

Facies		Sedimentary process	Description
A		Medium-energy hydric flow	Millimetric laminated sandy silt with some millimetric sand layers.
B		Low to medium-energy hydric flow	Millimetric lamination of silty clay with layers of fine sand.
C		Medium-energy hydric flow	Massive sandy silts.
D		Speleothem	Speleothem growth.
E		Sediment-gravity flow	Medium and fine sand without lamination.
F		Low-energy hydric flow/ sediment-gravity flow	Cemented lutites
G	G1	Medium-energy hydric flow	Massive silt with rip-up clasts of silt and clay.
	G2	Low-energy hydric flow	Massive clayed silt.
H		Medium-energy hydric flow	Centimetric lamination of clay, silt, and sand with a granular texture.

are sharps, and frequently facies B is found at the top (Fig. 13B and C). It has a plastic behavior under deformation stresses that causes folds and stretching. This facies can be compared with facies C of Gran Dolina's interior facies (Campaña et al., 2022), although with more silt and clay. This, with the fact that no rip-up clasts were found in Galería's facies C, suggests lesser energy in the formation of this facies than the facies C1 of the Gran Dolina site (Campaña et al., 2022). The sand laminates, which are rarely observed inside of this facies, could separate different events of deposits. The lack of internal structure suggests a relatively constant water flow and sediment input, also the horizontal deposition of the layers of this facies (in particular GIa.3, which is formed only by this facies) and its spatial relationship with facies B, which often appears on top of this facies, suggest that a slow flow formed this facies, but with more energy than facies B, as indicated by the grain size (a.3 in Fig. 7). Therefore, the facies association of facies B and Facies C would indicate a decreasing energy cycle.

Facies D: Speleothem (Fig. 13D). In GI, this facies is observed only in the SE section where a stalagmite is found in GIb.4 and speleothem crusts are found inside GIa.2. These layers are situated vertically in the same place, indicating a drip point in this area that indeed was active at the end of Early Pleistocene and, later, at the beginning of Middle Pleistocene, since both speleothems are situated at short distances above and below the Matuyama-Bruhnes paleomagnetism boundary. The drip point can be earlier since the section below GIa.2 is not known in this area, and there may be more speleothems or cementations at depth. A speleothem needs a sub-aerial condition with little or no detrital sedimentation. Therefore, a speleothem indicates vadose conditions (Springer and Kite, 1997) and a hiatus in the stratigraphic section (Gillieson, 1986).

Facies E: Massive 2.5Y 5/4 light olive brown medium and fine sand

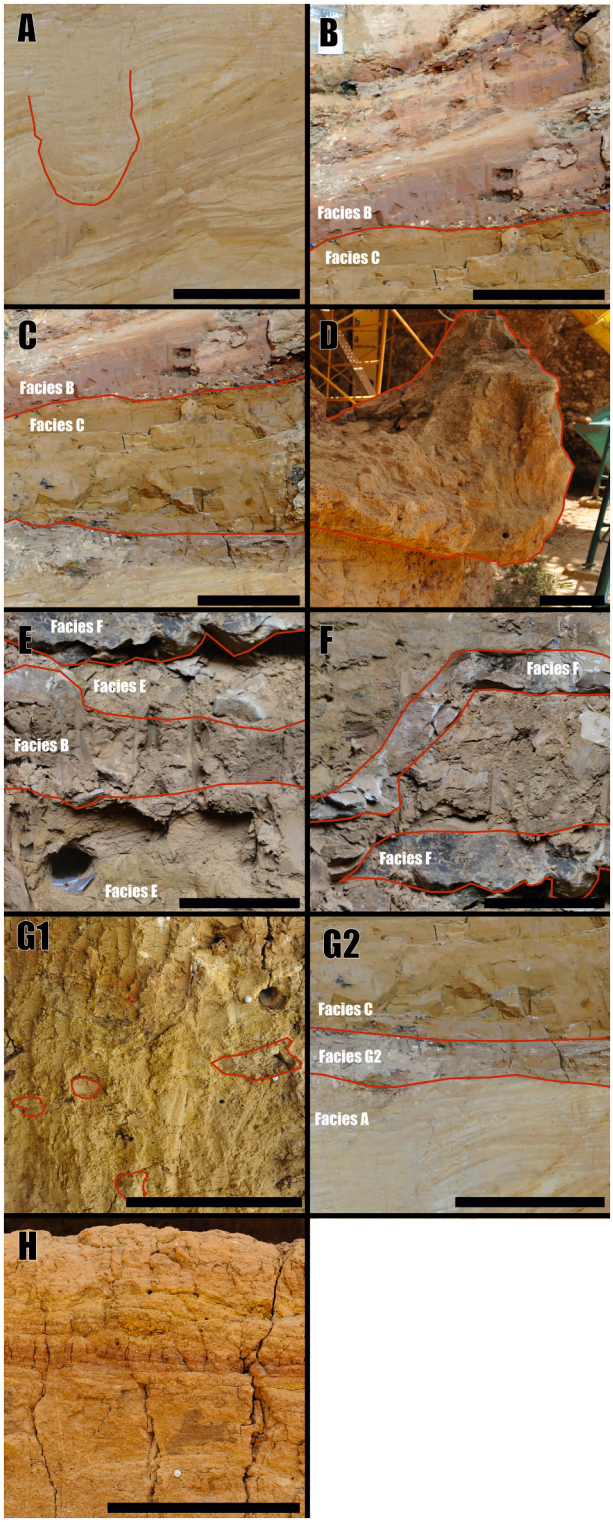

Fig. 13. Sedimentary facies of GI unit. (A) Facies A of GIa.5. Red line indicates a cut and fill. (B) Facies B of GIa.2 over the red line. (C) Facies C of GIa.3 marked by red lines. (D) Facies D of GIa.4. (E) Two layers of facies E of GIa.6. One under the red line and another at the top of the image surrounded by red lines. At the top of this image, calcilutites can be observed. (F) Two layers of facies F of GIa.6 are surrounded by red lines. The plastic deformation can be observed in the upper layer. (G1) Facies G1 of GIb.3 with rip-up clasts marked by red lines. (G2) Facies G2 of GIa.4 marked by red lines. (H) Facies H of GIb.1. The black bar represents 25 cm.

without lamination or internal structure (Fig. 13E) and can be classified as Sm (Miall, 1978). This facies has no >20 cm of thickness, and laterally it wedges at a few meters, with the top and base boundaries are sharps. This facies is only found in GIa.6 related to the facies B, C, and F, especially with the last that usually appears overlying facies E, indicating a genetic relationship. Similar to facies E has been defined in the Lapa Doce cave system as facies Sm (Laureano et al., 2016) and in Mugnano Cave as facies YS (Iacovello and Martini, 2012), which are interpreted as a sediment-gravity flow in an underground lake environment. The unsorted particle size, the lack of internal sedimentary structure, and the poor horizontal development of facies E (Fig. 13E) also suggest sediment-gravity flow for the formation of this deposit (Mulder and Alexander, 2001; Sakai et al., 2001; Dasgupta, 2003), similar to the Bouma A-division of a turbidity (Bouma, 1962). In that case, the genetic relationship with facies F has to be discussed. The lack of silt and clay in this layer suggests a subaqueous grain flow (Dasgupta, 2003), although their association with the F facies could suggest a subaqueous surge-like flow (Mulder and Alexander, 2001). Another possibility is that the sand may have lost the lamination due to post-depositional processes; therefore, this facies would have been deposited by a relatively medium-energy flow, but it is unlikely since other sand layers, as observed in GIa.5, maintain the planar lamination (Fig. 13A).

Facies F: Decimeter-thick cemented lutites. This facies is formed by cemented silt and clay, and it is mainly found in GIa.6, inside The Covacha de Los Zarpazos (Fig. 10), related to the facies E. The layers show folds associated with faults, which suggests post-depositional cementation of the layers, and breaks in a laminar manner (Fig. 13F). This facies has a few meters of lateral development, wedging laterally. The top and base boundaries are sharps.

This facies seems to be mainly formed by silt and clay, with a certain lamination preserved in the cementation, as the planar breakage suggests. Although the original dip of these layers is lost due to the post-depositional folding, the relationship with the underlying layers (formed by facies B and C), which shows horizontal lamination (Fig. 13B), suggests that facies F was deposited in a horizontal position. On one hand, one possible interpretation is that this facies is similar to facies B, which means mud is deposited by a low-energy hydrological flow that allows the settling of the suspended sediment that is subsequently cemented. On another hand, calcilutites have a limited extension since they are wedged in the current section, with an extension of no more than three meters, and they usually overlie the facies E, which may be interpreted as a sediment-gravity flow. These features can indicate that facies F was also formed by the sediment-gravity flow, representing this facies the fine sediment of the flow, which settle down after the deposit of the sediment-gravity flow, similar to a Bouma D-division of a turbidity flow (Bouma, 1962) or the upper level of a surge-like flow (Mulder and Alexander, 2001). This last interpretation must be taken carefully since post-depositional processes, such as folding and cementation, have been able to mask the sedimentary features.

Facies G: Massive 10YR 6/6 brownish-yellow to 10YR 6/4 light yellowish-brown silt and clay, mainly composed of quartz and phyllosilicates (Table 4). This facies shows sharps top and base boundaries. The most important characteristic of this facies is the lack of internal lamination, so can be classified as Fm (Miall, 1978). The layers of this facies can reach a thickness of about one meter. Depending on the presence of rip-up clasts, this facies is divided into two sub-facies.

Facies G1: Silt with rip-up clasts of silt and clay (Fig. 13G1). It is slightly folded and appears to fill erosive surfaces. This facies is mainly observed in GIb.3, GIb.5, and GIb.6.

Facies G2: Silt and clay without rip-up clasts (Fig. 13G2). The layers with this facies are usually thinner than facies G1, and they present plastic behavior that causes folding and stretching. It is observed in GIa.1, GIa.4, and GIb.2.

Since the facies G is massive, the sediments had to be deposited in a relatively constant environment. The rip-up clasts in facies G1 suggest

certain energy in the flow capable of eroding previous silt and clay sedimentary deposits, and that can drag larger particles than silt (Herman et al., 2012). The fact that only the silt fraction is dragged indicates that the source has not had larger particles available. This facies also appears to be filling erosional gaps suggesting that it is related to erosion events. Facies G2 is similar to the massive red clays of the top of the near Galería de las Arenas (Hernando-Alonso et al., 2022) and the slackwater facies defined by Bosch and White (2004). Both are explained as the result of a suspended load. In Sima Engañá (Málaga, Spain), similar facies to facies G2 is described in layer V and XIII and interpreted as the result of low-energy laminar flows (Cuenca et al., 2018). Therefore, facies G2 can be interpreted as the results of a suspended load during phreatic or epiphreatic conditions.

Facies H: Centimeter-sized lamination of different colors of clay, silt, and sand (Fig. 13H). This facies is only found in GIb.1, and it has a gentle dip through the south, where each lamina increases in thickness. The different centimeter-sized lamina has sharp boundaries among them, and the facies has sharp boundary at the top and base. Also, a granular texture is observed that, with the different particle size of the lamination and the dip, indicates that it is composed of reworked sediment. Therefore, this facies is formed by the erosion of previous deposits that explain the different sediment of the lamination. In this sense, this facies' lamination could be considered an inverse stratigraphy. The dip towards the southeast indicates a sink in this area, near the cave's south wall. This erosive event indicates that the conduit was in vadose conditions or in epiphreatic conditions. This facies represents the last deposit of GI.

The GI's stratigraphic section shows important variation in the sedimentology in the vertical and the horizontal. The different sedimentary facies indicate variations in the water table level and the hydrology of the karst system along the section (Fig. 3). The sedimentary facies A, B, and C, defined in this work, is similar to Gran Dolina facies of the same name, which have been interpreted as hydrological flow deposits in phreatic or epiphreatic conditions (Campaña et al., 2022). Most of these facies show planar and cross laminations that indicate a more or less constant water flow, both in phreatic and epiphreatic conditions (Springer and Kite, 1997). Also, the thickness of some layers, such as GIa.5, indicates a period with a water flow inside the cave, which agrees with temporary phreatic or epiphreatic conditions. Therefore, facies A, B, and C can be considered phreatic or epiphreatic facies; meanwhile, vadose conditions can be indicated by speleothems (facies D) and maybe the clearly erosive facies without lamination (facies G1 and facies H). Facies E and F can be interpreted as sediment-gravity flows; these facies can occur in phreatic, epiphreatic, and vadose conditions, but the primary horizontal position could indicate some water in the environment during the deposit, and also these facies are associated with facies C and B, that are considered as phreatic or epiphreatic facies; therefore, it is plausible to think that facies E and F are also phreatic or epiphreatic. In general, GI can be viewed as the result of an underground fluvial flow that transports sediments from farther sources than entrance facies.

4.2. Stratigraphy and sedimentology of the borehole

17 m thick sediments were recovered from the borehole about two meters from the Galería section (Fig. 14), in which several sedimentary changes were identified. The sequence of the borehole was described as follows: first, a one-meter anthropic fill composed on debris and heterogeneous sediments; second, a one-meter layer of fine sands surrounded by fragments of rocks that can be limestone clasts or cemented sediments, similar to the found at GIa.6; third, about two meters of clays with clast fragments that increases in size to the bottom; fourth, two meters of massive clays; and, finally, ten-meters of clayey sands (Fig. 14) (Bermejo et al., 2020). No sedimentary structure is observed in this sequence, but this may have been erased by drilling.

Because of its stratigraphic position, at about two meters in the SE section and with its top on the bottom of the Railway Trench, it can be assumed that the borehole belongs to GIa. In this area, the Galería section shows two speleothems and some cemented layers (Fig. 12). This may be indicated that this area (most central in the conduit) may be more affected by cementation than other areas of GI, so more cemented

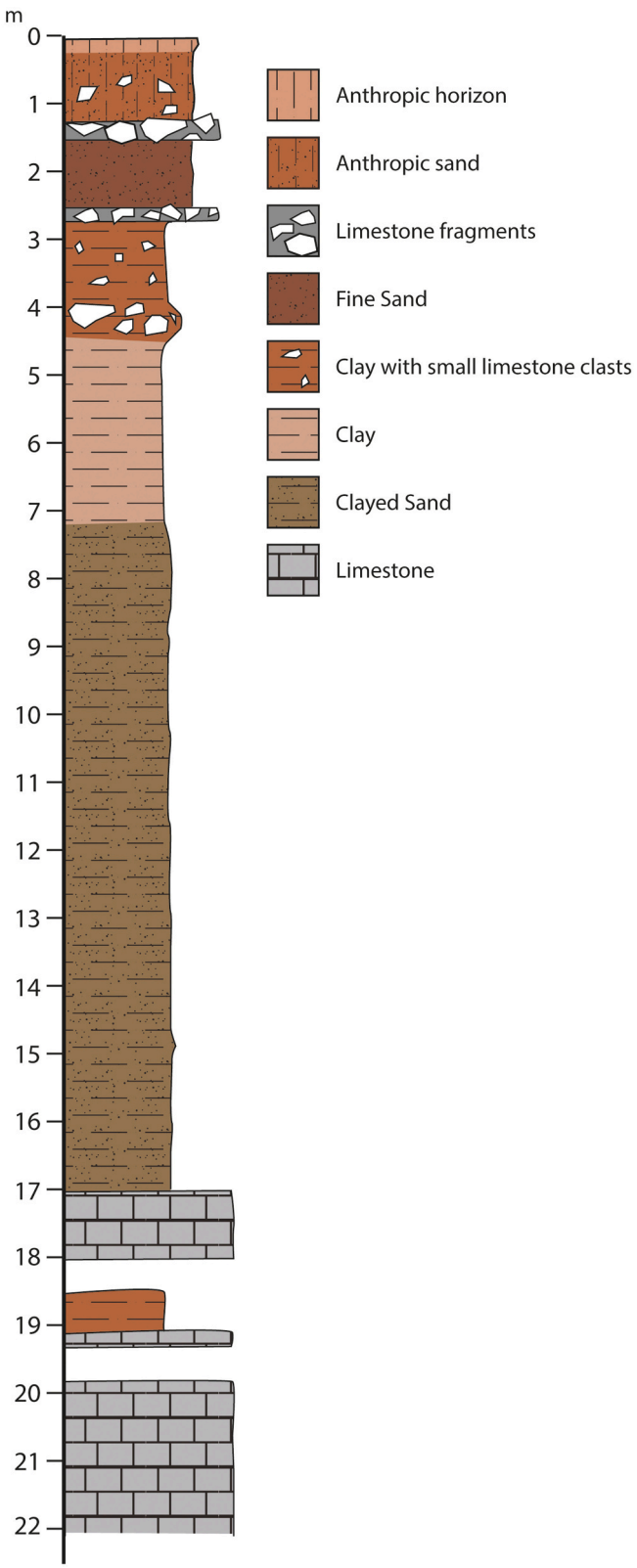

Fig. 14. Lithological description of Galería Complex borehole (Bermejo et al., 2020).

layers could be expected in depth. Considering this, the fragments of limestone described in the second layer of the borehole may be related to cemented layers and sands of GIa.2. Another possibility is that these fragments respond to anthropic fills from the railway or the quarrying activity of the near Compresor cave, but GPR profiles discouraged this possibility since anthropic structures have only been identified in the first-meter of depth in this location (Bermejo et al., 2020). GIa.3 has <20 cm in the SE section, and its lithology is not so different from the other layers to be noted in the borehole. The clays with clast fragments, situated in the borehole at ~3–4 m, may be GIa.5 with cemented layers or even GIa.6, although it would be unlikely that GIa.5 had little entity in the borehole since its thickness has remained more or less continuous in all the sections studied. The 2 m of clays and 10 m of clayey sands seem to be similar to GIa.5 and GIa.6 facies and, in the absence of a section in which the stratigraphic contacts can be appreciated, could be correlated to these layers.

4.3. Soft-sediments deformation structures

The soft-sediment deformation structures are defined as "deformations that occur in still unlithified sediments or in sedimentary rocks that had not yet undergone lithification before the deformation structures started to be formed." (van Loon, 2009). These structures have been widely described in quaternary environments, but their description in cave environments is scarce (Marean et al., 2004; Szczygiel et al., 2020). In GI, soft-sediment deformation structures are present in The Covacha de Los Zarpazos area, characterized by faults, fractures, and folds (Fig. 15).

The faults and fractures range from a few centimeters to >5 m. Five main faults have been observed in GI (Fig. 15). These are normal faults except for fault 2, which shows a reverse component. The vertical throw and dip angle of the faults can be found in Table 7.

The faults are sub-vertical, except for fault 1, which shows a dip between 18 and 5°. The fact that fault 2 and fault 3 have a similar gap and apparent dip angle, in addition to their closeness and morphology, indicates that they are the same fault that has an oblique direction with the stratigraphic sections. The fault has an angle of approximately 73° and is becoming more vertical towards the top.

Table 7
Vertical throw (in centimeters) and Apparent dip angle of the main faults of GI. The number of faults is indicated in Fig. 15.

Fault	Vertical throw	Apparent dip angle
1	20	18–5
2	70	90–84
3	60	90–73
4	25	83–74
5	100	90–85

The main faults distinguish in the section four blocks from the north to the south. The two lowest blocks are situated at the south-west, while the raised fault block is found east of The Covacha de Los Zarpazos (Fig. 15). In the last, the lowest part of the stratigraphic sequence of GI, the layer GIa.6 can be observed.

Rounded, low-amplitude anticlines and synclines form the folds of GI. These folds appear in layers with high content of silt and clay, as GIa.2 and GIa.3. Some folds are related to faults indicating that the sediment was very moist when the deformations occurred (Szczygiel et al., 2020).

In general, south and west dip is observed in GI. This dip is indeed post-depositional since most facies described show sedimentary features that suggest a horizontal deposit, such as horizontal lamination. The deformation and faults of GI do not affect the upper stratigraphic units of Galería (GII-GV), indicating that these occurred before the deposition of the exterior sediments.

5. Discussion

5.1. Interpretation of the facies, depositional environments of GI, and comparison with other caves

According to the borehole, GI has a thickness of about 17 m (Bermejo et al., 2020), in which only 6 m thick can be observed. Despite this, the sediments described in the borehole after the six meters show the same lithology, with 10 m thick of homogenous clayey sands (Fig. 14)

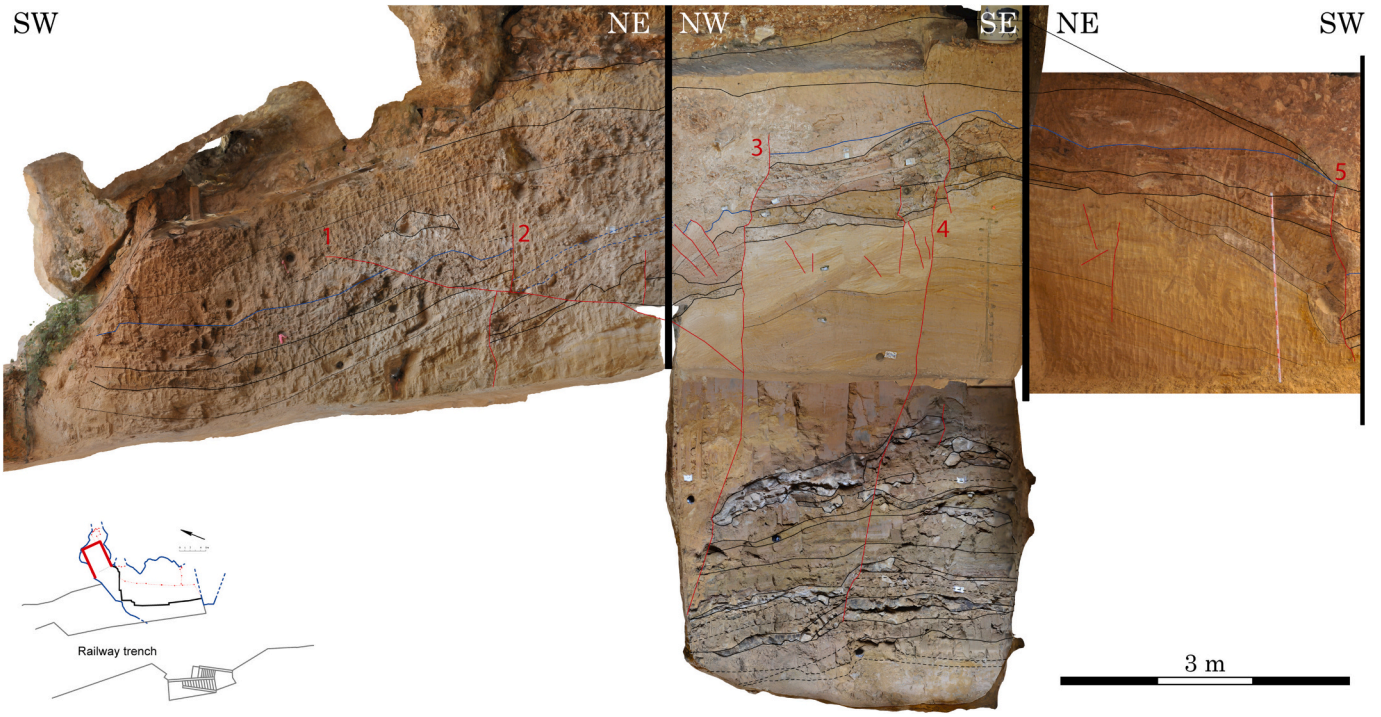

Fig. 15. GI stratigraphic section of Covacha de Los Zarpazos with the fractures and faults indicates in red lines.

(Bermejo et al., 2020), that may tentatively be correlated to GIa.6. Therefore, the study of the section should be enough to understand the main processes that happened in the cave during the Early and Middle Pleistocene (Fig. 16).

GIa.6 is formed by at least four cycles that show a decrease in the energy from massive sandy silts (facies C) to silty clay (facies B) and, after, a possible sediment-gravity flow represented by massive sands (facies E) and cemented lutites (facies F) on the top (Fig. 16). This can be interpreted as a drop in the water table that causes small collapses of the sediment. Thus, each cycle would indicate events of dropping in the water level, suggesting that the cave is in epiphreatic conditions at this moment. At the north of the Covacha de los Zarpazos, this layer has a vertical discordant boundary with GIa.5, which may be related to the fault observed in the upper levels, fault 3 (Fig. 9). An alternative explanation is an important erosion of this area and the later fill by GIa.5. The latter could explain the difference in the compaction and the later formation of the fault 3 in the overlying layers.

GIa.5 is a >3 m thick layer only formed by facies A (Fig. 16). This facies shows a millimetric lamination of sandy silt, with some cross lamination, partially eroded and fills (Figs. 13A and 10). The millimetric lamination suggests phreatic conditions inside the cave (Springer and Kite, 1997), but the erosion and fills indicate the drop of the water table during short times, therefore epiphreatic conditions. A possible alternative scenario involves a fluvial environment where periodic ponding occurs due to local blockages and shifting sediment. These features indicate complex hydrological dynamics inside the cave, with fluctuations in both energy and water table that could suggest that the cave continued in the epiphreatic zone at this moment.

After GIa.5, the sedimentation continued with layers of lesser thickness, suggesting more rapid changes in the hydrological conditions of the cave. Thus, GIa.4 is a small layer of clayey silt (facies G2) that, compared with GIa.5, suggests an energy drop in the system or less turbid water (Fig. 16). On top of this layer is GIa.3, formed by sandy silt of facies C, which can indicate an increase in the energy of the environment and stable phreatic conditions in the cave, and therefore a rise in the water table, which can be caused by internal sediment aggradation and blockage, in addition to external conditions.

GIa.2 is a complex layer mainly formed by millimetric layers of silty clay with layers of fine sands (facies B), with some speleothems (facies D) and cemented lutites (facies F) (Fig. 16). The facies B suggests a hydrological flow with minor energy changes. In the absence of a chronology frame, the millimetric changes of this facies may be due to relatively short-period environmental cycles. In Gran Dolina, similar lamination of interior facies has been explained as thousand-year cycles (Campaña et al., 2022). The speleothems in the south are lenticular-shaped horizontal layers 10–20 cm thick and are vertically related, suggesting a drip area that worked during at least two periods differently. The speleothem growths indicate the stop of other kinds of sedimentation and a relatively long period of time enough to grow the speleothem, in which the conduit would be in vadose conditions. In this part of the section, angular carbonate rock gravels are observed. These deposits can be small channels caused by fluvial flows that reworked cemented layers during vadose conditions. These changes seem to indicate rapid changes in the water table and the environment's energy, with periods of phreatic, epiphreatic and vadose conditions prolonged. This layer is found a few centimeters below the paleomagnetism boundary, interpreted as the Matuyama-Bruhnes boundary (Pérez-González et al., 2001), so its chronology may be slightly older than 780 ka.

GIa.1 is the last deposit of the Early Pleistocene, and it is formed by clayey silt interpreted as facies G2. It is difficult to follow because an erosion surface cuts it and its facies is very similar to the upper GIb deposits.

From GIb, the sedimentation changes in Galería Complex. This subunit is dominated by erosive processes and facies G1 that has rip-up clasts denoting reworking in the system. Planar- or cross-lamination are not observed. These features suggest changes in the hydrological conditions in the cave, from mainly epiphreatic conditions to vadose conditions (Fig. 16). This main change can be related to the final construction of the terrace T4 or the beginning of its incision in the hydrogeological basin of the Arlanzón River, which has an estimated age of about 0.85 Ma (Moreno et al., 2012; Benito-Calvo et al., 2017). This age is consistent with the paleomagnetism age proposed for the boundary between GIa and GIb (Pérez-González et al., 2001).

The sedimentation of GIb starts with GIb.6 and GIb.5, described as silt with rip-up clasts, and interpreted as facies G1. At the base of GIb.6, granular sediment of sand and fine, angular, matrix-supported gravel is found, indicating a reworking process. These layers would indicate the erosion of sub-aerial sediments in vadose conditions (Fig. 16).

The stalagmite overlying these two layers suggests vadose conditions and its thickness can indicate an important hiatus in the rest of the stratigraphic section.

Before the sedimentation of GIb.3, an important erosive process took place, affecting the levels from a.1 to a.5. This erosion is observed in the Galería section (Figs. 11 and 12), not being followed in Covacha de Los Zarpazos (Figs. 9 and 10). The erosion was after filled by GIb.3, which has rip-up clasts indicating the reworking of other layers; in fact, some of these rip-up clasts have been identified as a bit of facies B, which may be part of GIa.2. In this case, GIb.3 can be formed during the erosion process.

GIb.2 is a massive silt deposit without rip-up clast which has been interpreted as facies G2. The lack of lamination and concordance with GIb.3, would seem to indicate that it could be deposited at vadose conditions, although, in the absence of more features, an epiphreatic conditions cannot be rejected.

The last deposit of GI is GIb.1, formed by centimeter-sized lamination of different granular sediments (facies H), which is interpreted as a relativity medium-energy flow that reworked previous deposits (Figs. 13H and 12). In addition, some white beds with a few decimetres of lateral extension are found. There are non-cohesive beds that can be interpreted as small weathered speleothems. The dip of GIb.1 to the south indicates a possible low spot where the water drained away in this direction, which agrees with the morphology of GI and its paleo-surface since there is a clear southward trend marked by slope, erosion, and lower level thickness. This sinkhole, which suggests vadose conditions, may be active since the erosive event; in fact, the opening of this sinkhole can be caused by the erosive processes that eroded GIa and the bottom of GIb. Before this event, this draining spot may not have existed, and the waters from Galería flow in another direction, maybe to Gran Dolina cave or to another draining spot situated to the north in the railway cutting, where cave fillings were identified by the GPR survey (Bermejo et al., 2020). Unfortunately, no other flow direction indicators have been found in the cave. If this were so, the draining spot formation would be during the Middle Pleistocene and could be related to the formation of the lower level of the karst system, which has been associated with the Arlanzón terrace T5 (Ortega et al., 2013; Benito-Calvo et al., 2017). This terrace has an estimated age of about 660 ka (Moreno et al., 2012).

In sum, following the nine sedimentary facies described in this work (Table 6), GI can be separated into two depositional environments. First, the deposit of interior sediment during the Early Pleistocene in phreatic or epiphreatic conditions, related to the terrace T4 of Arlanzon River; and second, the erosion and reworking of this sediment during the Middle Pleistocene in vadose conditions.

5.2. *Soft-sediment deformation structure and erosion of the stratigraphic sequence*

The soft-sediment deformation structure in a cave is caused by post-depositional processes such as seismic movements, the collapse of the cave floor, erosion of the lower levels, or loss of volume of the underlying sediments due to desiccation or compaction, among others

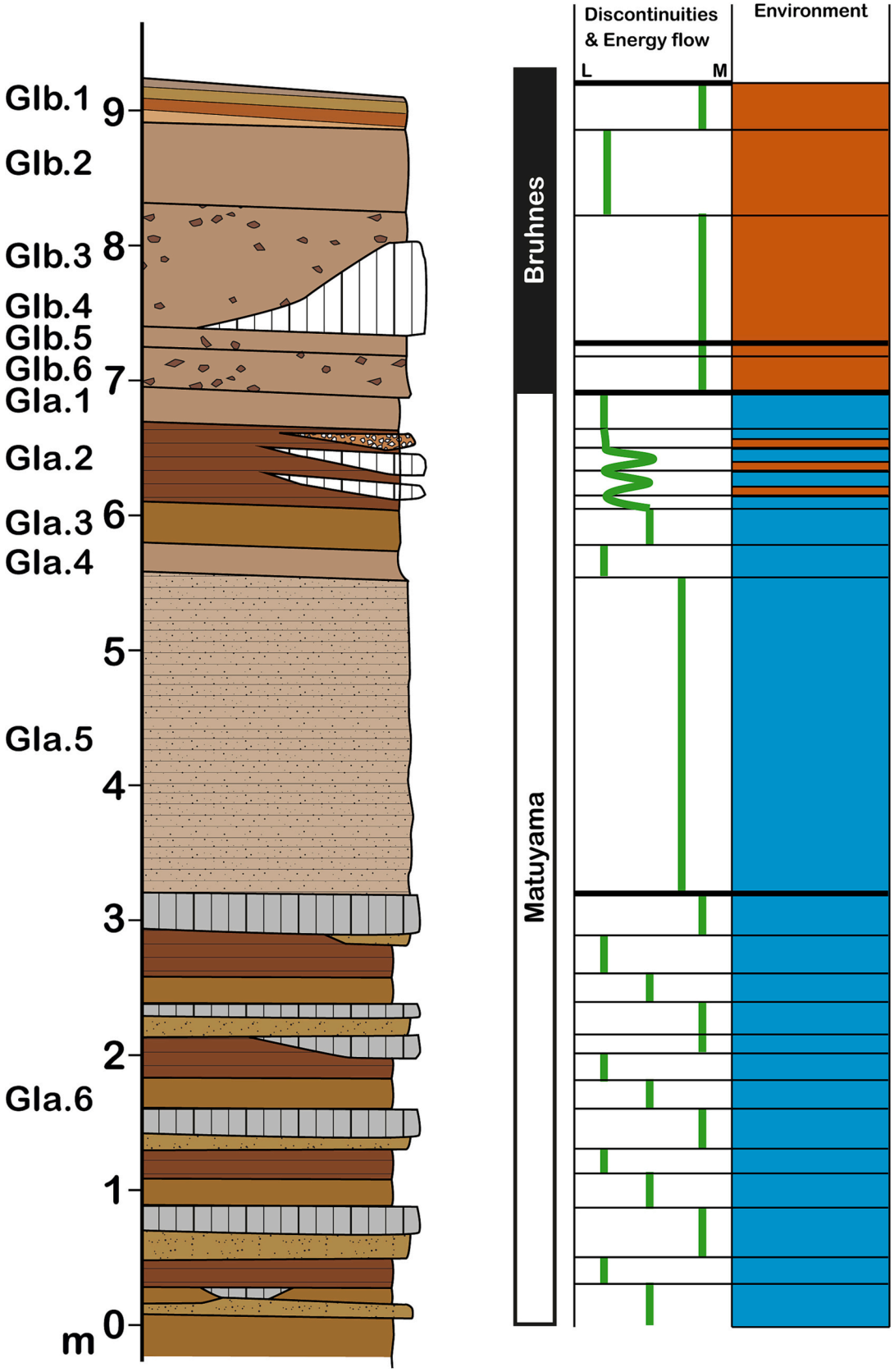

Fig. 16. Summary stratigraphic column, with all layers of GI. Discontinuities & Energy flow- Bold line: major discontinuity. Fine line: small discontinuity. L: Low energy. M: Medium energy. Environment- Blue: epiphreatic or phreatic conditions. Red: vadose conditions.

(Marean et al., 2004; van Loon, 2009). These kinds of faults and deformations have rarely been documented in other cave sediments (Marean et al., 2004; Bábek et al., 2015; Salomon et al., 2018; Szczygiel et al., 2020) and are generally explained as triggered by earthquakes or cryoturbation (Salomon et al., 2018).

Many soft-sediment deformation structures are observed in Galería Complex, most of them in the Covacha de Los Zarpazos, where brittle and plastic deformation found together suggests post-depositional processes in very moist sediments. In addition to the main faults, several small faults, including graben-like deformation (Fig. 15) and folds.

These deformations mainly affect the GIa sub-unit and the lower layers of GIb, except fault 5, which cuts the GIb.3 and GIb.2 layers and, therefore, occurred later (Fig. 15). This fault is also the one with the most significant gap, which may indicate that it was active during different events. In this sense, the soft-sediment deformation structure of the Galería Complex had to occur in the Middle Pleistocene.

Although earthquakes have been postulated as the cause of other deformation in caves (Salomon et al., 2018; Szczygiel et al., 2020), it is unlikely that it was the cause of Galería Complex because, on the one hand, the Sierra de Atapuerca is not in an active tectonic zone and, in the other hand, seismic movement indicators would be expected to be found in other caves of the karst system. In the nearby Gran Dolina cave, no feature has been described that can be associated with an earthquake; at the beginning of the Middle Pleistocene, a new entrance was opened in this cave, where the TD8 sediments entered (Campaña et al., 2017), but the erosion of the hillside can explain this opening. Significant fracturing has also been described at Cueva Peluda, which may be related to a seismic event (Ortega, 2009; Ortega et al., 2013), although the chronology is uncertain. Therefore, these deformations can be caused by the differential accommodation of the sediment, sediment erosion of the underlying layers, or a karstic collapse of the floor of the cave. According to the borehole, the sedimentation in-depth of the Galería Complex seems to be homogeneous, so the accommodation of the sediment was expected to be similar in all the conduit. However, there is an important lithological difference in the lower part of the Zarpazos, where cemented lutites are located in the lower part of the upper block, between faults 3 and 5 (Fig. 15). A possible explanation is that GIa.6 was partially eroded by a stream and subsequently filled by sediments from GIa.5. This difference in sediments would have caused compaction differences that would explain the formation of the soft sediment structures. This hypothesis would imply a significant erosion event between GIa.6 and GIa.5.

Other possible explanation is the main erosion event that eroded the top of GIa and the bottom of GIb. This erosion event was caused by the development of a drainage sink in the south of Galería, as the erosion surface, dipping to the south, indicates. The relationship between the erosion and the soft-sediment deformation structures is indicated by the fact that the faults and folds observed in the section seem only to affect the layers that are also affected by the erosion, with the exception as mentioned earlier of fault 5. In this case, it can be assumed that the faults, and surely the folding, were caused during this erosion event, which could erode underlying sediments, and caused material loss below the current stratigraphic section.

In terms of karstic collapse, geophysical prospection and current knowledge of the karst do not indicate the presence of a conduit beneath the Galería Complex (Ortega et al., 2013; Bermejo et al., 2020; Bermejo, 2021), although it has been described in other parts of the karst (Rosas et al., 2006).

To solve this problem, it would be necessary to advance in the excavation of the lower levels of GI.

5.3. Comparing Galería Complex and Gran Dolina

Gran Dolina site has 9 m of interior facies that have been separated into two lithostratigraphic units (TD1 and TD2) and into eight sedimentary facies (Campaña et al., 2022), which shows similar sedimentary features to the Galería Complex's facies defined in this work. The facies associations of Gran Dolina indicate a succession of phreatic and vadose phases that would define together epiphreatic conditions inside the cave, related to the transition between Arlanzón valley terraces T3 and T4. These hydrological changes have to be observed in Galería Complex sediments since these two caves belong to the same karst system (Ortega et al., 2013) and are <50 m from each other. Thus, a certain correlation between these two karstic fillings might be possible, but the chronology of both deposits shows certain differences; TD1 and TD2 of Gran Dolina have been dated in the Early Pleistocene; meanwhile, GI sediments have a date of Early and Middle Pleistocene (Pérez-González et al., 2001; Duval et al., 2022), although it should be noted that GI has only been dated by paleomagnetism, attempts with other techniques have been unsuccessful or have obtained inconsistent ages (Grün and Aguirre, 1987; Berger et al., 2008; Demuro et al., 2014), and that the lower 17 m of sediment is still undated. If we consider that these two conduits are connected, as the geophysical survey suggests (Bermejo et al., 2017), phreatic conditions in both caves are expected in the same period since the altitude of the caves are the same. TD1 unit of Gran Dolina was formed by the fluctuations in the water table level that caused the succession of phreatic and vadose phases (Campaña et al., 2022). According to the chronology, the phreatic conditions in Gran Dolina began shortly after the formation of the middle level of the karst (Duval et al., 2022); thus, similar conditions are expected in Galería too. Following this dissertation, an alternating flow between Gran Dolina and Galería could be possible so that GI deposits can have a chronology as old as the Gran Dolina sediments.

5.4. Geochemical analyses and geochronology implications

The mineralogy and elemental composition of the samples are very similar (Tables 4 and 5), and their difference can be explained by changes in the particle size, indicating that the source area has no change during the deposition of GI. This result is very similar to the mineralogy and elemental composition described in the interior sediments of TD1 and TD2 units of the Gran Dolina site (Campaña et al., 2022), suggesting the same source of the sediment.

One possible source of these sediments is the residue of the limestone. It occurs as sand, silt, and clay deposits with little or no evidence of fluvial transport and is sediment derived from insoluble residues in bedrock. Because it is slow to accumulate, it tends to be deposited in areas where there are no other sediment types, that is, in isolated areas or far away from external sediment inputs. The insoluble residue obtained from the Sierra de Atapuerca limestone is <0.1 g per kg and mainly composed of silt and clay (Aleixandre and Pérez-González, 1999). It is unlikely that the dissolution of the limestone is responsible for the 17 m of GI fill in Galería. Thus, it is probable that the sediment in Galería originates from a different source, potentially from the Arlanzón river or from soils of the Sierra de Atapuerca.

The sedimentary facies of the Galería Complex indicate a predominance of fluvial sediments in the interior of the karst. This seems to indicate that the source of the sediment would be a fluvial transport through the interior of the karst. Since the relationship of the Galería Complex with the rest of the karst in the Sierra de Atapuerca is unknown, the path that this sediment has taken inside the karst is also unknown, as is the entrance of these sediments into the karst. However, the southern contact between the Sierra de Atapuerca and the valley of the Arlanzón River was proposed as a potential entry for these sediments (Ortega and Martín-Merino, 2019).

The presence of crandallite was previously described in Galería Complex (Pérez-González et al., 1995; Demuro et al., 2014), and this mineral has been found in association with bat guano in other caves (Onac and Forti, 2011; Frost et al., 2012; Audra et al., 2019). According to the chemical analysis, it is present in most of the levels of GIa as a minor component (Tables 4 and 5). Crandallite is a phosphate that is formed under acidic conditions and is frequently found in open-air sites

but is less often found in caves (Karkanas et al., 2002). The formation of this mineral implies, on the one hand, acid conditions where the apatite is not stable; on another hand, the presence of this mineral in the sediment indicates a source of phosphorous in the system (Karkanas et al., 2000). Guano, wood ash, and dissolved bones have been postulated as possible sources of phosphorous in cave sediments (Schiegl et al., 1996; Karkanas et al., 2000, 2002). The sedimentary facies of GI suggest that no cave entrance was near when GI was deposited. In a close-cave environment is rare to find wood ash or bones, at least in sufficient quantity to provide as much phosphorous, and although bat guano is often found in this environment (Hill, 1999; Lewis, 2007; Marean et al., 2010), no bat guano deposit is described in GI. However, the preservation of the guano can be low due to its biological origin.

A possible source of the phosphorous may be the leaching from overlying layers of Galería. In the GII unit, a rich phosphorous layer is found that has been interpreted as a bat guano deposit (Pérez-González et al., 1995). The anomalous dates obtained in this unit have already been associated with their phosphate layers (Falguères et al., 2013). If it is the source, as Pérez-González et al. (1995) suggested, the fact that crandallite is found even in GIa.5, at a few meters below GII, suggests significant leaching in all GI units. This leaching may have entrained other elements besides phosphorus, such as uranium or thorium. The inputs of these elements would change the radioactivity of the sediment and can cause overestimated radiometric dose measurement. This could explain the anomalous chronological dates obtained for GIa, which has been dated by luminescence at 313 ± 19 ka and 310 ± 28 ka (Demuro et al., 2014) even though this sub-unit is found below the Matuyama-Bruhnesa boundary (Pérez-González et al., 2001), as has also been indicated to explain the anomalous dating values in GII (Falguères et al., 2013) and in Caune de l'Arago (Falguères et al., 2015).

In addition to the paleomagnetism chronology, the facies association of GI suggests hydrological changes inside the cave from mainly epiphreatic conditions to vadose conditions between GIa and GIb sub-units. As previously mentioned, this change could be related to the final construction of the terrace T4, dated by ESR with an estimated age of about 850 Ka (Moreno et al., 2012; Benito-Calvo et al., 2017). This suggests a chronology for GIa older than 850 ka.

6. Conclusions

The cave interior facies of the Sierra de Atapuerca has allowed the identification of the main hydrogeological changes in the sedimentation of the middle level of the karst system and its geomorphological evolution. This work presents a complete study of the internal facies of the Galeria Complex, which is one of the best stratigraphic sections for studying the cave interior facies.

GI unit is 19 m thick of interior facies in the base of Galería Complex, of which 6 m thick can be observed in the section, while the rest is described in a borehole drilled two meters from the section. The unit is separated into two sub-units, GIa and GIb, by a paleomagnetism boundary interpreted as the Matuyama-Bruhnes boundary. This separation was done following chronostratigraphic criteria, and the sedimentology study supports it because these two sub-units show different sedimentological features that denote different depositional environments. Thus, the GIa sub-unit is dominated by facies that indicate a hydrological flow in the conduits under epiphreatic conditions (facies A, B, C, E, and F) during the Early Pleistocene; meanwhile, GIb shows important erosion events and facies with reworked materials (facies G and H) that indicate vadose conditions during the Middle Pleistocene. This environmental change can be related to the final construction of the terrace T4 in the hydrogeological basin of the Arlanzón River.

The most important erosion event occurred before the sedimentation of GIb.3, affecting the underlying layers. This erosion event could be caused by the opening of a draining spot in the south of Galería during the Middle Pleistocene, which had to be active until at least the end of GI.

Four main faults have been described in The Covacha de Los Zarpazos area that separated four blocks. They show high angles near 90° and a throw between 20 cm to 100 cm. Associated with these faults, numerous minor faults and folds can be observed. These soft-sediment deformation structures of the Galería Complex can be one of the best examples of this kind of structure described in caves.

The possible connection between of Gran Dolina cave and the Galería Complex, and the similarity of their sedimentary facies suggest that the sedimentation in Galería Complex has to be related, and, therefore, GI deposits may potentially have a chronology as old as Gran Dolina sediments. Nevertheless, the dates obtained in GIa show an anomalous chronology, about 310 ka, that does not correspond with paleomagnetic or sedimentological data. The presence of phosphates in all the sediments of GI analyzed suggests significant leaching of elements in this unit, indeed from GII bat guano deposit. This leaching may have entrained other elements in addition to phosphorus, such as uranium or thorium, that can cause changes in the radioactivity of the environment and explain the underestimated ages obtained in other works.

Declaration of competing interest

The authors declare that they have no known competing financial interests or personal relationships that could have appeared to influence the work reported in this paper.

Data availability

Data will be made available on request.

Acknowledgments

This study was supported by the project PGC2018-093925-B-C31 and PID2021-122355NB-C33 financed by MCIN/AEI/10.13039/501100011033/FEDER, UE. I. Campaña is the beneficiary of a post-doctoral grant from Junta de Andalucía. Fieldwork at Atapuerca is supported by the Consejería de Cultutra y Turismo of the Junta de Castilla y León. This work has benefited from discussion with Lucía Bermejo and two anonymous reviewers.

Appendix A. Supplementary data

Supplementary data to this article can be found online at https://doi.org/10.1016/j.geomorph.2023.108864.

References

Aleixandre, T., Pérez-González, A., 1999. Facies mineralógicas de las arenas de los rellenos kársticos de la Sierra de Atapuerca (Burgos). In: Andreo, B., Carrasco, F., Durán, J.J. (Eds.), Contribución del estudio científico de las cavidades kársticas al conocimiento geológico, pp. 231–242.

Álvarez-Posada, C., Parés, J.M., Cuenca-Bescós, G., Van der Made, J., Rosell, J., Bermúdez de Castro, J.M., Carbonell, E., 2018. A post-Jaramillo age for the artefact-bearing layer TD4 (Gran Dolina, Atapuerca): new paleomagnetic evidence. Quat. Geochronol. 45, 1–8.

Arnold, L.J., Demuro, M., Parés, J.M., Pérez-González, A., Arsuaga, J.L., Bermúdez de Castro, J.M., Carbonell, E., 2015. Evaluating the suitability of extended-range luminescence dating techniques over early and Middle Pleistocene timescales: published datasets and case studies from Atapuerca, Spain. Quat. Int. 389, 167–190.

Arriolabengoa, M., Iriarte, E., Aranburu, A., Yusta, I., Arrizabalaga, A., 2015. Provenance study of endokarst fine sediments through mineralogical and geochemical data (Lezetxiki II cave, northern Iberia). Quat. Int. 364, 231–243. https://doi.org/10.1016/j.quaint.2014.09.072.

Arsuaga, J.L., Martínez, I., Lorenzo, C., Gracia, A., Muñoz, A., Alonso, O., Gallego, J., 1999. The human cranial remains from Gran Dolina Lower Pleistocene site (Sierra de Atapuerca, Spain). J. Hum. Evol. 37 (3–4), 431–457.

Audra, P., De Waele, J., Bentaleb, I., Chroňáková, A., Krištůfek, V., D'Angeli, I.M., Carbone, C., Madonia, G., Vattano, M., Scopelliti, G., Cailhol, D., Vanara, N., Temovski, M., Bigot, J.-Y., Nobécourt, J.-C., Galli, E., Rull, F., Sanz-Arranz, A., 2019. Guano-related phosphate-rich minerals in European caves. Int. J. Speleol. 48 (1), 75–105.

Auler, A.S., Smart, P.L., Wang, X., Piló, L.B., Edwards, R.L., Cheng, H., 2009. Cyclic sedimentation in Brazilian caves: mechanisms and palaeoenvironment significance. Geomorphology 106, 142–153.

Bábek, O., Briestenský, M., Precechtelová, G., Stepancíková, P., Hellstrom, J.C., Drysdale, R.N., 2015. Pleistocene speleothem fracturing in the foreland of the Western Carpathians: a case study from the seismically active eastern margin of the Bohemian Massif. Geol. Q. 59, 491–506. https://doi.org/10.7306/gq.1225.

Benito-Calvo, A., Pérez-González, A., 2015. Geomorphology of the Sierra de Atapuerca and the Middle Arlanzón Valley (Burgos, Spain). J. Maps 11 (4), 535–544. https://doi.org/10.1080/17445647.2014.909339.

Benito-Calvo, A., Pérez-González, A., Parés, J.M., 2008. Quantitative reconstruction of Late Cenozoic landscapes: a case study in the Sierra de Atapuerca (Burgos, Spain). Earth Surf. Process. Landf. 33 (2), 196–208.

Benito-Calvo, A., Ortega, A.I., Pérez-González, A., Campaña, I., Bermúdez de Castro, J. M., Carbonell, E., 2017. Palaeogeographical reconstruction of the Sierra de Atapuerca Pleistocene sites (Burgos, Spain). Quat. Int. 433, 379–392. https://doi.org/10.1016/j.quaint.2015.10.034.

Benito-Calvo, A., Ortega, A.I., Navazo, M., Moreno, D., Pérez-Gonzalez, A., Parés, J.M., Bermúdez De Castro, J.M., Carbonell, E., 2018. Pleistocene geodynamic evolution of the Arlanzón valley: implications for the formation of the endokarst system and the open air archaeological sites of the Sierra de Atapuerca (Burgos, España). Bol. Geol. Min. 129, 059–082.

Berger, G.W., Pérez-González, A., Carbonell, E., Arsuaga, J.L., Bermúdez de Castro, J.M., Ku, T.L., 2008. Luminescence chronology of cave sediments at the Atapuerca palaeoanthropological site, Spain. J. Hum. Evol. 55, 300e311.

Bermejo, L., 2021. Reconocimiento de morfologías endokársticas y yacimientos en los karst de la Sierra de Atapuerca y Ojo Guareña (Burgos) mediante técnicas de prospección geofísica. Ph.D Thesis.. University of Burgos, Spain.

Bermejo, L., Ortega, A.I., Guérin, R., Benito-Calvo, A., Pérez-González, A., Parés, J.M., Aracil, E., Bermúdez de Castro, J.M., Carbonell, E., 2017. 2D and 3D ERT imaging for identifying karst morphologies in the archaeological sites of Gran Dolina and Galería Complex (Sierra de Atapuerca, Burgos, Spain). Quat. Int. 433, 393–401.

Bermejo, L., Ortega, A.I., Parés, J.M., Campaña, I., Bermúdez de Castro, J.M., Carbonell, E., Conyers, L.B., 2020. Karst features interpretation using ground-penetrating radar: a study from the Sierra de Atapuerca, Spain. Geomorphology 367, 1–14.

Bermúdez de Castro, J.M., Martinón-Torres, M., Arsuaga, J.L., Carbonell, E., 2017. Twentieth anniversary of Homo antecessor (1997-2017). Evol. Anthropol. 26 (4), 157–171.

Blott, S.J., Pye, K., 2012. Particle size scales and classification of sediment types based on particle size distributions: review and recommended procedures. Sedimentology 59 (7), 2071–2096.

Bosch, R., White, W.B., 2004. Lithofacies and transport of clastic sediments in karstic aquifers. In: Sasowsky, I.D., Mylroie, J., Bosch, R., White, W.B. (Eds.), Studies of Cave Sediments. Springer, Dordrecht, pp. 1–22.

Bouma, A.H., 1962. Sedimentology of Some Flysch Deposits. Elsevier, Amsterdam, p. 168.

Bull, P.A., 1981. Some fine-grained sedimentation phenomena in caves. Earth Surf. Process. Landf. 6 (1), 11–22.

Campaña, I., 2018. Estratigrafía y sedimentología del yacimiento de Gran Dolina (Sierra de Atapuerca, Burgos). Ph.D Thesis.. University of Burgos, Spain.

Campaña, I., Benito-Calvo, A., Pérez-González, A., Bermúdez de Castro, Carbonell, E., 2016. Assessing automated image analysis of sand grain shape to identify sedimentary facies, Gran Dolina archaeological site (Burgos, Spain). Sediment. Geol. 346, 72–83. https://doi.org/10.1016/j.sedgeo.2016.09.010.

Campaña, I., Benito-Calvo, A., Pérez-González, A., Ortega, A.I., Bermúdez de Castro, J. M., Carbonell, E., 2017. Pleistocene sedimentary facies of the Gran Dolina archaeo-paleoanthropological site (Sierra de Atapuerca, Burgos, Spain). Quat. Int. 433, 68–84. https://doi.org/10.1016/j.quaint.2015.04.023.

Campaña, I., Benito-Calvo, A., Pérez-González, A., Álvaro-Gallo, A., Miguens-Rodríguez, L., Iglesias-Cibanal, J., Bermúdez de Castro, J.M., Carbonell, E., 2022. Revision of TD1 and TD2 stratigraphic sequence of Gran Dolina cave (Sierra de Atapuerca, Spain). J. Iber. Geol. 48, 425–443.

Carbonell, E., Bermúdez De Castro, J.M., Parés, J.M., Pérez-González, A., Cuenca-Bescós, G., Ollé, A., Mosquera, M., Huguet, R., Van Der Made, J., Rosas, A., Sala, R., Vallverdú, J., García, N., Granger, D.E., Martinón-Torres, M., Rodríguez, X.P., Stock, G.M., Vergès, J.M., Allué, E., Burjachs, F., Cáceres, I., Canals, A., Benito, A., Díez, C., Lozano, M., Mateos, A., Navazo, M., Rodríguez, J., Rosell, J., Arsuaga, J.L., 2008. The first hominin of Europe. Nature 452 (7186), 465–469.

Chung, F.H., 1975. Quantitative interpretation of X-Ray diffraction patterns. III. Simultaneous determination of a set of reference intensities. J. Appl. Crystallogr. 8–1, 17–19.

Creer, K.M., Kopper, J.S., 1976. Secular oscillations of the geomagnetic field recorded by sediments deposited in caves in the Mediterranean Region. Geophys. J. Int. 45 (1), 35–58. https://doi.org/10.1111/j.1365-246X.1976.tb00312.x.

Cuenca, J.J., Robledo, P.A., Durán, J.J., Pardo-Igúzquiza, E., Cheng, H., Martos, S., Luque, J.A., Moreno, L., 2018. Paleoclimatic inferences from the study of a sedimentary sequence alternating detrital sediments and speleothmes in Sima Engañá, Sierra de las Nieves (Málaga). Cuaternario Geomorfol. 32 (1–2), 75–89. https://doi.org/10.17735/cyg.v32i1-2.56659.

Dasgupta, P., 2003. Sediment gravity flow – the conceptual problems. Earth Sci. Rev. 62, 265–281.

Demuro, M., Arnold, L.J., Parés, J.M., Pérez-González, A., Ortega, A.I., Arsuaga, J.L., Bermúdez de Castro, J.M., Carbonell, E., 2014. New luminescence ages for the Galería Complex archaeological site: resolving chronological uncertainties on the Acheulean record of the Sierra de Atapuerca, Northern Spain. PLoS ONE 9 (10).

Duval, M., Grün, R., Parés, J.M., Martín-Francés, L., Campaña, I., Rosell, J., Shao, Q., Arsuaga, J.L., Carbonell, E., Bermúdez de Castro, J.M., 2018. The first direct ESR dating of a hominin tooth from Atapuerca Gran Dolina TD-6 (Spain) supports the antiquity of *Homo antecessor*. Quat. Geochronol. 47, 120–137.

Duval, M., Arnold, L.J., Demuro, M., Parés, J.M., Campaña, I., Carbonell, E., Bermúdez de Castro, J.M., 2022. New chronological constraints for the lowermost stratigraphic unit of Atapuerca Gran Dolina (Burgos, N Spain). Quat. Geochronol. 71, 101292 https://doi.org/10.1016/j.quageo.2022.101292.

Falguères, C., Bahain, J.J., Yokoyama, Y., Arsuaga, J.L., Bermudez De Castro, J.M., Carbonell, E., Bischoff, J.L., Dolo, J.M., 1999. Earliest humans in Europe: the age of TD6 Gran Dolina, Atapuerca, Spain. J. Hum. Evol. 37 (3–4), 343–352.

Falguères, C., Bahain, J.-J., Bischoff, J.L., Pérez-González, A., Ortega, A.I., Ollé, A., Quiles, A., Ghaleb, B., Moreno, D., Dolo, J.-M., Shao, Q., Vallverdú, J., Carbonell, E., Bermúdez de Castro, J.M., Arsuaga, J.L., 2013. Combined ESR/U-series chronology of Acheulian hominid-bearing layers at Trinchera Galería site, Atapuerca, Spain. J. Hum. Evol. 65, 168–184.

Falguères, C., Shao, Q., Han, F., Bahain, J.J., Richard, M., Perrenoud, C., Moigne, A.M., Lumley de, H., 2015. New ESR and U-series dating at Caune de l'Arago, France: a key-site for European Middle Pleistocene. Quat. Geochronol. 30B, 547–553.

Farrand, W.R., 1975. Sediment analysis of a prehistoric rockshelter: the Abri Pataud. Quat. Res. 5, 1–26.

Farrand, W.R., 2001. Sediments and stratigraphy in rockshelters and caves: a personal perspective on principles and pragmatics. Geoarchaeology - Int. J. 16 (5), 537–557.

Forbes, M.S., Bestland, E.A., 2007. Origin of the sedimentary deposits of the Naracoorte Caves, South Australia. Geomorphology 86, 369–392.

Ford, D.C., Williams, P., 2007. Karst Hydrogeology and Geomorphology. John Wily and Son, Ltd.

Fornós, J.J., Ginés, J., Gràcia, F., 2009. Present-day sedimentary facies in the coastal karst caves of Mallorca island (western Mediterranean). J. Cave Karst Stud. 71 (1), 86–99.

Frost, R.L., Palmer, S.J., Pogson, R.E., 2012. Thermal stability of crandallite $CaAl_3(PO_4)_2(OH)_5{\cdot}(H_2O)$ a 'Cave' mineral from the Jenolan Caves. J. Therm. Anal. Calorim. 107 (3), 905–909.

Gil, E., Aguirre, E., Hoyos, M., 1987. Contexto Estratigráfico. In: Aguirre, E., Carbonell, E., Bermúdez de Castro, J.M. (Eds.), El hombre fósil de Ibeas y el Pleistoceno de la Sierra de Atapuerca. Junta de Castilla y León.

Gillieson, D., 1986. Cave sedimentation in the New Guinea highlands. Earth Surf. Process. Landf. 11, 533–543.

Goldberg, P., Sherwood, S.C., 2006. Deciphering human prehistory through the geoarchaeological study of cave sediments. Evol. Anthropol. 15, 20–36.

Grün, R., Aguirre, E., 1987. Datación por ESR y por la serie de1 U, en los depósitos cársticos de Atapuerca. In: Aguirre, E., Carbonell, E., Bermúdez de Castro, J.M. (Eds.), El Hombre Fósil de Ibeas y el Pleistoceno de la Sierra de Atapuerca. Junta de Castilla y León, Valladolid, pp. 201–204.

Herman, E.K., Toran, L., White, W.B., 2012. Clastic sediment transport and storage in fluviokarst aquifers: an essential component of karst hydrogeology. Carbonates Evaporites 27, 211–241.

Hernando-Alonso, I., Moreno, D., Ortega, A.I., Benito-Calvo, A., Alonso, M.J., Parés, J.M., Martínez-Fernández, A., Carbonell, E., Bermúdez de Castro, J.M., 2022. ESR chronology of the fluvial sequence of Cueva del Silo (Sierra de Atapuerca, Spain). Quat. Geochronol. 73, 101374.

Hill, C.A., 1999. Mineralogy of Kartchner caverns, Arizona. J. Cave Karst Stud. 61 (2), 73–78.

Iacovello, F., Martini, I., 2012. Provenance and geological significance of red mud and other clastic sediments of the Mugnano Cave (Montagnola Senese, Italy). Int. J. Speleol. 41 (2), 317–328.

Kadlec, J., Chadima, M., Lisá, L., Hercman, H., Osintsev, A., Oberhänsli, H., 2008. Clastic cave deposits in botovskaya cave (Eastern Siberia, Russian federation). J. Cave Karst Stud. 70 (3), 142–155.

Kampolis, I., Triantafyllidis, S., Skliros, V., Kamperis, E., 2022. Quaternary evolutionary stages of Selinitsa Cave (SW Peloponnese, Greece) reveal sea-level changes based on 3D scanning, geomorphological, biological, and sedimentological indicators. Quaternary 5, 24. https://doi.org/10.3390/quat5020024.

Karkanas, P., Bar-Yosef, O., Goldberg, P., Weiner, S., 2000. Diagenesis in prehistoric caves: the use of minerals that form in situ to assess the completeness of the archaeological record. J. Archaeol. Sci. 27 (10), 915–929.

Karkanas, P., Rigaud, J.P., Simek, J.F., Albert, R.M., Weiner, S., 2002. Ash Bones and guano: a study of the minerals and phytoliths in the sediments of Grotte XVI, Dordogne, France. J. Archaeol. Sci. 29 (7), 721–732.

Kaufmann, G., Romanov, D., Nielbock, R., Lundberg, J., 2020. The sediment record of the Unicorn Cave, southern Harz Mountains, Germany. Geomorphology 367, 107295.

Kukla, J., Lozek, V., 1958. K. problematica vyzkumu jeskynnich vyplni (concerning the problems of the investigation of cave sediments). Ceskoslov. Kras. 2, 19–83.

Kurečić, T., Bočić, N., Wacha, L., Bakrač, K., Grizelj, A., Tresić Pavičić, D., Lüthgens, C., Sironić, A., Radović, S., Redovniković, L., Fiebig, M., 2021. Changes in cave sedimentation mechanisms during the Late Quaternary: an example from the lower Cerovačka Cave, Croatia. Front. Earth Sci. 9, 672229 https://doi.org/10.3389/feart.2021.672229.

Laureano, F.V., Karmann, I., Granger, D.E., Auler, A.S., Almeida, R.P., Cruz, F.W., Strícks, N.M., Novello, V.F., 2016. Two million years of river and cave aggradation in NE Brazil: implications for speleogenesis and landscape evolution. Geomorphology 273, 63–77.

Lewis, H., 2007. Preliminary soil micromorphology studies of landscape and occupation history at Tabon Cave, Palawan, Philippines. Geoarchaeology 22 (7), 685–708.

Macken, A.C., McDowell, M.C., Bartholomeusz, D.N., Reed, E.H., 2013. Chronology and stratigraphy of the Wet Cave vertebrate fossil deposit, Naracoorte, and relationship

to paleoclimatic conditions of the Last Glacial Cycle in south-eastern Australia. Aust. J. Earth Sci. 60 (2), 271–281. https://doi.org/10.1080/08120099.2013.758657.
Marean, C.W., Nilssen, P.J., Brown, K., Jerardino, A., Stynder, D., 2004. Paleoanthropological investigations of Middle Stone Age sites at Pinnacle Point, Mossel Bay (South Africa): archaeology and hominid remains from the 2000 field season. J. Paleoanthropol. 2, 14–83.
Marean, C.W., Bar-Matthews, M., Fisher, E., Goldberg, P., Herries, A., Karkanas, P., Nilssen, P.J., Thompson, E., 2010. The stratigraphy of the Middle Stone Age sediments at Pinnacle Point Cave 13B (Mossel Bay, Western Cape Province, South Africa). J. Hum. Evol. 59 (3–4), 234–255.
Martín-Francés, L., Martinón-Torres, M., Martínez de Pinillos, M., García-Campos, C., Zanolli, C., Bayle, P., Modesto-Mata, M., Arsuaga, J.L., Bermúdez de Castro, J.M., 2020. Crown tissue proportions and enamel thickness distribution in the Middle Pleistocene hominin molars from Sima de los Huesos (SH) population (Atapuerca, Spain). PLoS ONE 15 (6), e0233281. https://doi.org/10.1371/journal.pone.0233281.
Martini, I., 2011. Cave clastic sediments and implications for speleogenesis: new insights from the Mugnano Cave (Montagnola Senese, Northern Apennines, Italy). Geomorphology 134 (3–4), 452–460.
Martini, I., Ronchitelli, A., Arrighi, S., Capecchi, G., Ricci, S., Scaramucci, S., Spagnolo, V., Gambassini, P., Moroni, A., 2018. Cave clastic sediments as a tool for refining the study of human occupation of prehistoric sites: insights from the cave site of La Cala (Cilento, southern Italy). J. Quat. Sci. 33 (5), 586–596.
Martín-Merino, M.A., Domingo, S., Antón, T., 1981. Estudio de las cavidades de la zona BU-IV A (Sierra de Atapuerca). Kaite 2, 41–76.
Martín-Perea, D.M., Maíllo-Fernández, J.M., Marín, J., Arroyo, X., Asiaín, R., 2022. A step back to move forward: a geological re-evaluation of the El Castillo Cave Middle Palaeolithic lithostratigraphic units (Cantabria, northern Iberia). J. Quat. Sci. 38 (2), 221–234.
Miall, A.D. (Ed.), 1978. Fluvial Sedimentology. xii + 859 pp. Canadian Society of Petroleum Geologists Memoir 5. Calgary. ISBN 0 920230 03 2.
Moreno, D., Falguères, C., Pérez-González, A., Duval, M., Voinchet, P., Benito-Calvo, A., Ortega, A.I., Bahain, J.J., Sala, R., Carbonell, E., Bermúdez de Castro, J.M., Arsuaga, J.L., 2012. ESR chronology of alluvial deposits in the Arlanzón valley (Atapuerca, Spain): contemporaneity with Atapuerca Gran Dolina site. Quat. Geochronol. 10, 418–423. https://doi.org/10.1016/j.quageo.2012.04.018.
Moreno, D., Falguères, C., Pérez-González, A., Voinchet, P., Ghaleb, B., Despriée, J., Bahain, J.-J., Sala, R., Carbonell, E., Bermúdez de Castro, J.M., Arsuaga, J.L., 2015. New radiometric dates on the lowest stratigraphical section (TD1 to TD6) of Gran Dolina site (Atapuerca, Spain). Quat. Geochronol. 30, 535–540.
Mulder, T., Alexander, J., 2001. The physical character of subaqueous sedimentary density flows and their deposits. Sedimentology 48, 269–299.
Núñez-Lahuerta, C., Galán, J., Cuenca-Bescós, G., García-Medrano, P., Cáceres, I., 2022. A bird assemblage across the MIS 9/8 boundary: the Middle Pleistocene of Galería (Atapuerca). Quat. Sci. Rev. 293, 107708.
Ollé, A., Cáceres, I., Vergès, J.M., 2005. Human occupation at Galería site (Sierra de Atapuerca, Burgos, Spain) after the technological and taphonomical data. In: Molinea, N., Moncel, M.H., Monnier, J.-L. (Eds.), Les premiers peuplements en Europe, BAR International Series, S1364. John and Erika Hedges Ltd., Oxford, pp. 269–280.
Ollé, A., Mosquera, M., Rodríguez, X.P., de Lombera-Hermida, A., García-Antón, M.D., García-Medrano, P., Peña, L., Menéndez, L., Navazo, M., Terradillos, M., Bargalló, A., Márquez, B., Sala, R., Carbonell, E., 2013. The Early and Middle Pleistocene technological record from Sierra de Atapuerca (Burgos, Spain). Quat. Int. 295, 138–167.
Onac, B., Forti, 2011. Minerogenetic mechanisms occurring in the cave environment: an overview. Int. J. Speleol. 40 (2), 79–98.
Ortega, A.I., 2009. La Evolución Geomorfológica del karst de la Sierra de Atapuerca (Burgos) y su relación con los yacimientos pleistocenos que contiene. Universidad de Burgos, Facultad de Humanidades y Educación. Departamento de ciencias históricas y geografía.
Ortega, A.I., Martín, M.A., 2023. In press Hypogenic Origin of the Sierra de Atapuerca Karst (Burgos, Spain). Abstract Book- Diputación Provincial Burgos, pp. 44–47.
Ortega, A.I., Martín-Merino, M.A., 2019. La terraza del sondeo de la Cantera Cudillo (La Paredeja) y su posible relación con la de Cueva del Silo, Cueva Peluda y Trinchera Elefante. Cubía 23, 54–56.
Ortega, A.I., Benito-Calvo, A., Pérez-González, A., Martín, M.Á., Pérez, R., Parés, J.M., Aramburu, A., Arsuaga, J.L., Bermúdez de Castro, J.M., Carbonell, E., 2013. Evolution of multilevel caves in the Sierra de Atapuerca (Burgos, Spain) and its relation to human occupation. Geomorphology 196, 122–137.
Ortega, A.I., Benito-Calvo, A., Pérez-González, A., Carbonell, E., Bermúdez de Castro, J. M., Arsuaga, J.L., 2014. Atapuerca karst and its palaeoanthropological sites. In: Gutiérrez, F., Gutiérrez, M. (Eds.), Landscapes and Landforms of Spain, World Geomorphological Landscapes, pp. 101–110.
Ortega, A.I., Benito-Calvo, A., Martín, M.A., Pérez-González, A., Parés, J.M., Bermúdez de Castro, J.M., Arsuaga, J.L., Carbonell, E., 2018. Las cuevas de la Sierra de Atapuerca y el uso humano del paisaje kárstico durante el Pleistoceno (Burgos, España). Bol. Geol. Min. 129 (1/2), 83–105.
Osborn, R.A.L., 1984. Lateral facies changes, unconformities and stratigraphic reversals: their significance for cave sediment stratigraphy. In: Cave Science. Transactions British Cave Research Association, 11(3).
Parés, J.M., Pérez-González, A., 1995. Paleomagnetic age for hominid fossils at Atapuerca archaeological site, Spain. Science 269, 830–832.
Parés, J.M., Pérez-González, A., 1999. Magnetochronology and stratigraphy at Gran Dolina section, Atapuerca (Burgos, Spain). J. Hum. Evol. 37, 325–342.
Parés, J.M., Ortega, A.I., Benito-Calvo, A., Aranburu, A., Arsuaga, J.L., Bermúdez de Castro, J.M., Carbonell, E., 2016. Paleomagnetic constraints on the Atapuerca karst development (N Spain). Geol. Soc. Am. Spec. Pap. 516.
Parés, J.M., Álvarez, C., Sier, M., Moreno, D., Duval, M., Woodhead, J.D., Ortega, A.I., Campaña, I., Rosell, J., Bermúdez de Castro, J.M., Carbonell, E., 2018. Chronology of the cave interior sediments at Gran Dolina archeological site, Atapuerca (Spain). Quat. Sci. Rev. 186, 1–16.
Pérez-González, A., Aleixandre, T., Pinilla, A., Gallardo, J., Benayas, J., Martínez, M.J., 1995. Aproximación a la estratigrafía de galería en la trinchera de la Sierra de Atapuerca (Burgos). In: Bermúdez de Castro, J.M., Arsuaga, J.L., Carbonell, E. (Eds.), Evolución humana en Europa y los yacimientos de la Sierra de Atapuerca, pp. 99–122.
Pérez-González, A., Parés, J.M., Gallardo, J., Aleixandre, T., Ortega, A.I., Pinilla, A., 1999. Geología y estratigrafía del relleno de Galería de la Sierra de Atapuerca (Burgos). In: Carbonell, E., Rosas, A., Díez, C. (Eds.), ATAPUERCA: Ocupaciones humanas y paleoecología del yacimiento de Galería, pp. 31–42.
Pérez-González, A., Parés, J.M., Carbonell, E., Aleixandre, T., Ortega, A.I., Benito-Calvo, A., Martín-Merino, M.A., 2001. Géologie de la Sierra de Atapuerca et stratigraphie des remplissages karstiques de Galería et Dolina (Burgos, Espagne). L'Anthropologie 105 (1), 27–43.
Rodríguez, J., Burjachs, F., Cuenca-Bescós, G., García, N., Van der Made, J., Pérez González, A., Blain, H.-A., Expósito, I., López-García, J.M., García Antón, M., Allué, E., Cáceres, I., Huguet, R., Mosquera, M., Ollé, A., Rosell, J., Parés, J.M., Rodríguez, X.P., Díez, C., Rofes, J., Sala, R., Saladié, P., Vallverdú, J., Bennasar, M.L., Blasco, R., Bermúdez de Castro, J.M., Carbonell, E., 2011. One million years of cultural evolution in a stable environment at Atapuerca (Burgos, Spain). Quat. Sci. Rev. 30 (11–12), 1396–1412.
Rodríguez-Gómez, G., Palmqvist, P., Martínez-Navarro, B., Martín-González, J.A., Bermúdez de Castro, J.M., 2022. Mean body size estimation in large mammals and the computation of biomass in past ecosystems: an application to the Pleistocene sites of Orce and Sierra de Atapuerca (Spain). C. R. - Palevol. 2022 (10), 207–233. https://doi.org/10.5852/cr-palevol2022v21a10.
Rosas, A., Bermúdez de Castro, J.M., 1999. The ATD6-5 mandibular specimen from Gran Dolina (Atapuerca, Spain). Morphological study and phylogenetic implications. J. Hum. Evol. 37 (3–4), 567–590.
Rosas, A., Huguet, R., Pérez-González, A., Carbonell, E., Bermúdez de Castro, J.M., Vallverdú, J., Van der Made, J., Allué, E., García, N., Martínez-Pérez, R., Rodríguez, J., Sala, R., Saladié, P., Benito-Calvo, A., Martínez-Maza, C., Bastir, M., Sánchez, A., Parés, J.M., 2006. The "Sima del Elefante" cave site at Atapuerca (Spain). Estud. Geol. 62 (1), 327–348.
Sakai, T., Yokokawa, M., Kubo, Y., Endo, N., Masuda, F., 2001. Grain fabric of experimental gravity flow deposits. Sediment. Geol. 154, 1–10.
Salomon, M.L., Grasemann, B., Plan, L., Gier, S., Schöpfer, M.P.J., 2018. Seismically-triggered soft-sediment deformation structures close to a major strike-slip fault system in the Eastern Alps (Hirlatz cave, Austria). J. Struct. Geol. 110, 102–115. https://doi.org/10.1016/j.jsg.2018.02.010.
Santonja, M., Pérez-González, A., 2018. Sobre la definición en clave exclusivamente achelense del yacimiento de Galería (Atapuerca, Burgos). In: Boletín del Seminario de Arte y Arqueología, arqueología LXXXIV, pp. 5–53.
Santonja, M., Pérez-González, A., 2021. Review of the Acheulean component of the lithic industry from Galería (Atapuerca, Burgos, Spain). Trab. Prehist. 78 (1), 26–48. https://doi.org/10.3989/tp.2021.12263.
Schiegl, S., Goldberg, P., Bar-Yosef, O., Weiner, S., 1996. Ash deposits in Hayonim and Kebara Caves, Israel: macroscopic, microscopic and mineralogical observations, and their archaeological implications. J. Archaeol. Sci. 23 (5), 763–781.
Springer, G.S., Kite, J.S., 1997. River-derived slackwater sediments in caves along Cheat River, West Virginia. Geomorphology 18, 91-00.
Šroubek, P., Diehl, J.F., Kadlec, J., 2007. Historical climatic record from flood sediments deposited in the interior of Spirálka Cave, Czech republic. Palaeogeogr. Palaeoclimatol. Palaeoecol. 251 (3–4), 547–562.
Stratford, D., Clark, L.J., Wojcieszak, M., Wadley, L., d'Errico, F., de la Peña, P., Esteban, I., Sievers, C., Banks, W.E., Beard, T., Horn, M., Shadrach, K., Morrisey, P., Mauran, G., Bacwell, L., 2022. Quat. Sci. Rev. 291, 107618.
Szczygiel, J., Wróblewski, W., Mendecki, M.J., Hercman, H., Bosák, P., 2020. Soft-sediment deformation structures in cave deposits and their possible causes (Kalacka Cave, Tatra Mts. Poland). J. Struct. Geol. 140, 104161.
Valen, V., Lauritzen, S.E., Løvlie, R., 1997. Sedimentation in a high-latitude karst cave: Sirijordgrotta, Nordland, Norway. Nor. Geol. Tidsskr. 77, 233–250.
van Loon, A.J., 2009. Soft-sediment deformation structures in siliciclastic sediments: an overview. Geologos 15, 3–55.
White, W.B., 2007. Cave sediments and paleoclimate. J. Cave Karst Stud. 69 (1), 76–93.
Zazo, C., Goy, J.L., Hoyos, M., 1987. Contexto geológico y geomorfológico. In: Aguirre, E., Carbonell, E., Bermúdez de Castro, J.M. (Eds.), El hombre fósil de Ibeas y el Pleistoceno de la Sierra de Atapuerca. Junta de Castilla y León, Soria.